UNCLASSIFIED

AD 274 076

Reproduced
by the

ARMED SERVICES TECHNICAL INFORMATION AGENCY
ARLINGTON HALL STATION
ARLINGTON 12, VIRGINIA

UNCLASSIFIED

NOTICE: When government or other drawings, specifications or other data are used for any purpose other than in connection with a definitely related government procurement operation, the U. S. Government thereby incurs no responsibility, nor any obligation whatsoever; and the fact that the Government may have formulated, furnished, or in any way supplied the said drawings, specifications, or other data is not to be regarded by implication or otherwise as in any manner licensing the holder or any other person or corporation, or conveying any rights or permission to manufacture, use or sell any patented invention that may in any way be related thereto.

A-62-3-1
NOX

CATALOGED BY ASTIA
AS AD No. 274 076

AFCRL-62-155

REPORT 1116-16

IONOSPHERIC STUDIES USING POLARIZATION ROTATION OF SATELLITE RADIO SIGNALS

BY

BYRON C. POTTS

ANTENNA LABORATORY
DEPARTMENT OF ELECTRICAL ENGINEERING
THE OHIO STATE UNIVERSITY RESEARCH FOUNDATION
COLUMBUS 12, OHIO

Scientific Report #11
Contract AF 19(604)-7270
Project 4649
Task 46490

APR 2 1962

Research
Initiated and Sponsored by

DETECTION PHYSICS LABORATORY
ELECTRONICS RESEARCH DIRECTORATE
AIR FORCE CAMBRIDGE RESEARCH LABORATORIES
OFFICE OF AEROSPACE RESEARCH
UNITED STATES AIR FORCE
BEDFORD, MASSACHUSETTS

24 JANUARY 1962

NOTICES

When Government drawings, specifications, or other data are used for any purpose other than in connection with a definitely related Government procurement operation, the United States Government thereby incurs no responsibility nor any obligation whatsoever, and the fact that the Government may have formulated, furnished, or in any way supplied the said drawings, specifications, or other data, is not to be regarded by implication or otherwise as in any manner licensing the holder or any other person or corporation, or conveying any rights or permission to manufacture, use, or sell any patented invention that may in any way be related thereto.

The Government has the right to reproduce, use, and distribute this report for governmental purposes in accordance with the contract under which the report was produced. To protect the proprietary interests of the contractor and to avoid jeopardy of its obligations to the Government, the report may not be released for non-governmental use such as might constitute general publication without the express prior consent of The Ohio State University Research Foundation.

Qualified requesters may obtain copies of this report from the ASTIA Document Service Center, Arlington Hall Station, Arlington 12, Virginia. Department of Defense contractors must be established for ASTIA services, or have their "need-to-know" certified by the cognizant military agency of their project or contract.

AFCRL-62-155 REPORT 1116-16

IONOSPHERIC S. JDIES USING POLARIZATION ROTATION OF SATELLITE RADIO SIGNALS

BY

BYRON C. POTTS

ANTENNA LABORATORY
DEPARTMENT OF ELECTRICAL ENGINEERING
THE OHIO STATE UNIVERSITY RESEARCH FOUNDATION
COLUMBUS 12, OHIO

Scientific Report #11
Contract AF 19(604)-7270
Project 4649
Task 46490

Research
Initiated and Sponsored by

DETECTION PHYSICS LABORATORY
ELECTRONICS RESEARCH DIRECTORATE
AIR FORCE CAMBRIDGE RESEARCH LABORATORIES
OFFICE OF AEROSPACE RESEARCH
UNITED STATES AIR FORCE
BEDFORD, MASSACHUSETTS

24 JANUARY 1962

NOTICES

a. Inside the cover, on the back of the title page, or on a separate sheet following the title page of all reports except those containing classified RESTRICTED DATA, the following information shall be displayed.

"Requests for additional copies by Agencies of the Department of Defense, their contractors, and other Government agencies should be directed to the:

ARMED SERVICES TECHNICAL INFORMATION AGENCY
ARLINGTON HALL STATION
ARLINGTON 12, VIRGINIA

Department of Defense contractors must be established for the ASTIA servies or have their "need-to-know" certified by the cognizant military agency of their project or contract."

b. Unclassified reports shall also display the following additional information: "All other persons and organizations should apply to the:

U.S. DEPARTMENT OF COMMERCE
OFFICE OF TECHNICAL SERVICES
WASHINGTON 25, D.C."

ABSTRACT

The polarization rotation is studied for radio signals received from an artificial satellite in the ionosphere. A first-order analysis is used which leads to values for the integrated electron density in the ionosphere. These values are compared with those calculated by other means and with those obtained by other investigators. A new parameter, the rate of polarization null position, is introduced as a method for obtaining the electron density at satellite altitudes. The methods employed in the analysis are outlined and additional means of improving the analysis are discussed.

LIST OF SYMBOLS

(All units rationalized MKS where not specified)

N_H = electron content in a column of height h_s and 1 square meter in area

f = frequency in cycles per second

h_s = height of the satellite in meters

V = velocity in meters per second

T = Faraday rotation null period in seconds, $T = \frac{\pi}{d\theta/dt}$

E = electric field of an electromagnetic wave

e = electronic charge

B = magnetic field density in webers per meter^2

μ_o = permeability of free space

H = magnetic field intensity in amperes per meter

F = force in Newtons

m = mass of an electron

t = time in seconds

r = instantaneous distance from the satellite to the point of observation, i.e., range

ω = $2\pi f$

ω_H = angular gyromagnetic resonance frequency, $2\pi f_H$

ω_o = angular plasma frequency, $2\pi f_o$

N = number density of electrons in electrons per meter^3

ϵ_o = permittivity of free space

γ = propagation constant (appendix only)

θ = polarization rotation due to the Faraday effect in radians

S = length of the mean propagation path in meters

ψ = angle subtended at the earth's center by r

D = electric flux density

ϕ = angle between the magnetic field vector and the direction of propagation

ds = element of actual propagation path length

dr = element of optical path length

dh = element of height normal to the earth's surface

ξ = angle between the direction of propagation and the zenith at the satellite

K_1 = constant equal to 2.97×10^{-2}, rationalized MKS units

K_2 = constant equal to 2.39, rationalized MKS units

i = zenith angle of the propagation path at the earth observation point

M = $H \cos \phi \sec \xi$ for a flat earth, $H \cos \phi \sin(i - \xi)/(\sin i - \sin \xi)$ for a spherical earth

M_s = value of M at the satellite

C = velocity of light in a vacuum

f_c = critical frequency at h_m

h_m = height of the maximum of the F_2 layer = h_{max}

$\overline{M}$ = mean value of M (see Appendix V)

$\frac{d\theta}{dt}$ = time rate of change of the Faraday polarization rotation

N_s = number density of electrons at the satellite height

H_s = magnitude of the magnetic field at the satellite height

H^s = scale height (usually in kilometers)

N_o = H_{max} = electron density at the maximum of the F_2 layer

ϕ_s = angle between the magnetic field and the direction of propagation at the satellite

Y = correction factor for neglecting higher order terms in the binomial expansion for θ (main body of the report only)

$X_o = f_c^2/f^2$

$SH_{max} = \int_0^{h_m} N\,dh$, integrated electron density to h_m

N_{HP} = integrated electron density to h_s computed from satellite positions a minute apart assuming the $dN/dh \approx 0$

N_{TH} = theoretical value of the integrated electron density to h_s based on an assumed distribution N(h)

R = N_a/N_b = ratio of ionization above F_2 max to that below

Y = height of the equidensity column having density N_{max} and total content $N_H - SH_{max}$.

TABLE OF CONTENTS

		Page
A.	INTRODUCTION	1
B.	THE FARADAY ROTATION OF SINGLE-FREQUENCY SATELLITE RADIO SIGNALS	2
	1. The First-Order Faraday Effect	2
	2. The Faraday-Rate of Rotation	5
	3. Second-Order Faraday Rotation	6
C.	PHYSICAL PARAMETERS AND CORRECTIONS TO THE THEORY	7
	1. Physical Quantities and Relationships	7
	2. Corrections and Discussion of the Theory	15
	3. The Two-Point High Pass Approximation	19
D.	EXPERIMENTAL RESULTS	20
	1. Integrated Electron Density to the Satellite	20
	2. Ionization above the F_2 Layer Maximum	25
	3. Equivalent Heights of the Ionosphere	26
	4. The Effect of Magnetic Disturbance on N_H	26
	5. The Integrated Electron Density from Longer Periods of Observation	26
	6. First Order Determination of N_S	31
E.	CONCLUSIONS AND RECOMMENDATIONS	34
ACKNOWLEDGEMENTS		35
REFERENCES		36

APPENDIX I - DERIVATION OF THE PROPAGATION CONSTANT FOR AN IONIZED MEDIUM 41

APPENDIX II - DERIVATION OF THE FARADAY ROTATION EXPRESSIONS UNDER THE QUASI-LONGITUDINAL AND QUASI-TRANSVERSE CONDITIONS 46

1. Longitudinal and Quasi-Longitudinal Propagation 46

2. Transverse and Quasi-Transverse Propagation 49

APPENDIX III - GEOMETRY OF A SATELLITE PASS 52

APPENDIX IV - AN EXPANSION OF THE EARTH'S MAGNETIC FIELD 57

APPENDIX V - DISCUSSION OF THE MEAN VALUES $\overline{M}, h_M$ 63

APPENDIX VI - EXPERIMENTAL EQUIPMENT 65

IONOSPHERIC STUDIES USING POLARIZATION ROTATION OF SATELLITE RADIO SIGNALS

A. INTRODUCTION

As an artificial earth satellite travels through the ionized atmosphere of the earth, the detectability of the object may be altered by its interaction with the ionosphere. The magnitude of this effect is related to the density of the electrons at satellite altitudes. It is, therefore, of interest to study the electron content in the upper ionosphere in order to be able to assign realistic values to theoretical models of satellite-ionospheric interaction as well as to form a sound experimental basis for the theory of formation of the complete ionosphere.

Many methods have been used to measure the number density of electrons lying above the maximum of the F_2 layer: radio star refraction,[1] Faraday polarization rotation of lunar reflected radio signals,[2] polarization rotation of artificial earth satellite radio signals,[3-8] satellite doppler measurements,[9] radio absorption measurements,[10] radio refraction measurements,[11] dispersive doppler measurements,[12] direct measurements, by National Aeronautics and Space Administration,[13] and various experiments using rockets and satellites.[14, 15] A rather complete historical record of the early work is given by Evans,[16] who also covers the radar backscatter observation methods. All the above methods have yielded results as to the electron density in the upper ionosphere, but the accuracy of the results is often ambiguous. This ambiguity arises chiefly from two factors: (1) the ionosphere, a virtual sea of moving particles, must usually be treated as a "quiet" spherically stratified region in order to interpret results, and (2) many approximations and assumptions must be made in analyzing the results (e.g., approximating the ray path of a radio signal in the ionosphere). These measurement techniques, however, are continually being improved, and this report is primarily concerned with some new insights into the method of analyzing the rate of polarization rotation of a satellite signal in order to gain more accurate electron content values in the upper ionosphere.

Polarization rotation of a radio signal was first used to study the ionosphere by Brown[2] et al in lunar reflection measurements. This

group set down the first order equation to determine the electron content. Bowhill,[17] soon after the advent of artificial satellites, reported that the rate of rotation is, under certain assumptions, constant for a given direction of satellite motion. Bauer and Daniels[4] set down improved equations for studying the Faraday polarization rotation and rate of polarization rotation under more general satellite geometries and at two observation points. This work was closely paralleled by that of Arendt.[18] Extensive measurements using the Faraday rotation method have been reported by Hame and Stuart,[3] Garriott,[19] Little and Lawrence,[7] and Yeh and Swenson.[8] These measurements have provided preliminary data on the total electron content of the ionosphere, its dirurnal and seasonal variations, the effects of spurious solar activity, and the extent of large-scale irregularities.

This Laboratory has worked on the measurement of ionospheric electron densities since the advent of earth satellites, primarily through the work of Hame.[20] The radio signals of earth satellite 1958Δ2 (Sputnik III) were used in order to obtain rate of polarization rotation measurements which led to early results[3,21] concerning the electron density in the ionosphere. Models of the electron distribution above the F_2 layer maximum were later published by Hame and Stuart.[22,23] The present report uses the 19.9904 Mc radio signal of 1959 Iota I (Explorer VII) to continue this previous work with a more accurate calculation of the integrated electron density. A study of the feasibility of obtaining electron densities at the satellite altitude is also described.

B. THE FARADAY ROTATION OF SINGLE-FREQUENCY SATELLITE RADIO SIGNALS

1. The First-Order Faraday Effect

The relationship between the Faraday polarization rotation of a radio signal originating within the ionosphere and the number density of electrons in the ionosphere is given by the equation:

$$(1) \qquad \theta = \frac{K_1}{f^2} \int_0^S NH \cos\phi \, ds + \frac{K_2}{f^4} \int_0^S N^2 H \cos\phi \, ds + \cdots .$$

The details of the derivation of Eq. (1) are given in Appendices I and II. Several major assumptions are implicit in Eq. (1): the gyromagnetic frequency, f_H, and the critical frequency, f_o, are assumed much smaller than the signal frequency, the quasi-longitudinal condition of propagation must exist (see Appendix II), and the ionosphere is

assumed to be spherically stratified. If the further assumption is made that the frequency f is high enough that the higher order terms in Eq. (1) can be neglected, then the polarization rotation is given simply by

$$\theta = \frac{K_1}{f^2} \int_0^S NH \cos \phi \, ds. \tag{2}$$

An alternative form of Eq. (2) which is useful instanteously is

$$\theta = \frac{K_1}{f^2} \int_0^{h_s} NH \cos \phi \sec \xi \, dh \tag{3}$$

where it is assumed that $ds = \sec \xi \, dh$; this is the same as assuming an optical path and a flat earth since the real relationship between an optical path length and the satellite height for a spherical earth is shown in Fig. 1, and is given by

$$ds = \frac{\sin(i-\xi)}{\sin i - \sin \xi} \, dh. \tag{4}$$

Using Eq. (4), a first order form for the spherical earth is

$$\theta = \frac{K_1}{f^2} \int_0^{h_s} NH \cos \phi \, \frac{\sin(i-\xi)}{\sin i - \sin \xi} \, dh. \tag{5}$$

In deriving Eqs. (3) and (5) from Eq. (2) it is important to remember that no refraction or path splitting of the satellite signal as it passes through the ionosphere is taken into account.

Equation (3) and Eq. (5) are useful since they allow integration in the direction normal to the earth's surface. Since the number density of electrons is assumed to depend only on the altitude, h, it is convenient to put Eq. (3) and Eq. (5) into the approximate form

$$\theta = \frac{K_1}{f^2} \, \overline{M} \int_0^{h_s} N \, dh \tag{6}$$

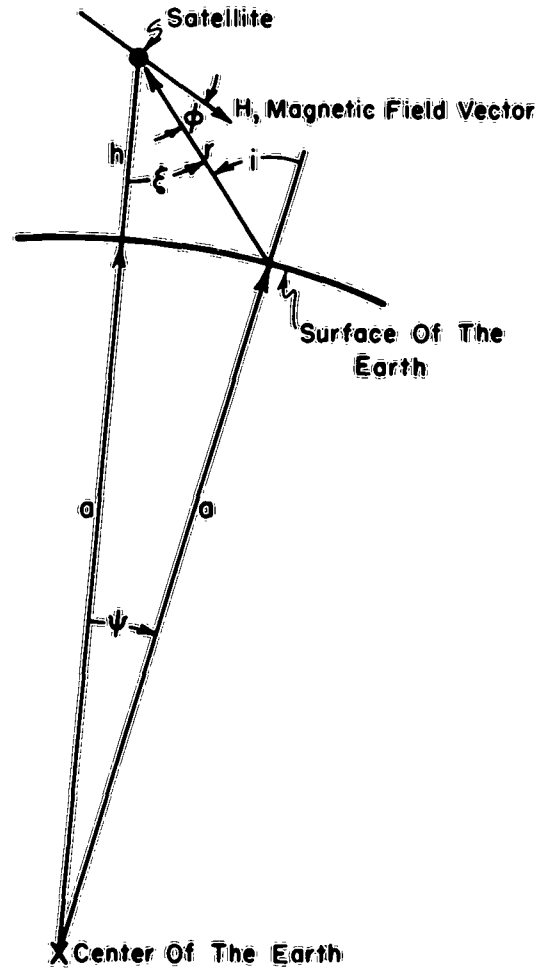

Fig. 1. Geometry of a satellite pass.

where $\bar{M}$ is the mean value of other factors under the integral in Eq. (3) and Eq. (5). Obviously, $\bar{M}$ will be slightly different for the flat earth and spherical earth cases, but both are of interest in dealing with satellite passages where the closest point of approach is quite close to the observing site. The details of evaluating $\bar{M}$ are discussed in Appendix V, as well as the electron density distribution assumed in applying the mean value theorem.

Since the integrated electron density is usually of interest, Eq. (6) can be written as

$$N_H \equiv \int_0^{h_s} N\, dh = \frac{\theta f^2}{\bar{M} K_1} \tag{7}$$

where θ is found experimentally and yields an experimental value for N_H under all the assumptions made in developing Eq. (7).

2. The Faraday-Rate of Rotation

The use of the polarization method in the form of Eq. (7) has limited use because of the ambiguity of the number of rotations of θ at a single frequency. It is necessary, therefore, to examine an alternate method, namely the time rate of change of the polarization rotation of a satellite radio signal. The mathematical expression is given by differentiation of Eq. (2) which yields

$$(8) \quad \frac{d\theta}{dt} = \frac{K_1}{f^2} \left\{ \int_0^S N \frac{\partial}{\partial t} (H \cos \phi) ds + \int_0^S H \cos \phi \frac{\partial N}{\partial t} ds + N_s H_s \cos \phi_s \frac{ds}{dt} \right\} .$$

Another form, assuming an optical ray path, is the derivative of Eq. (6), and is

$$(9) \quad \frac{d\theta}{dt} = \frac{K_1}{f^2} \left\{ \frac{\partial \bar{M}}{\partial t} \int_0^{h_s} N \, dh + \bar{M} \int_0^{h_s} \frac{\partial N}{\partial t} dh + \bar{M} N_s \frac{dh_s}{dt} \right\} .$$

The most useful form of the rate of rotation, however, is given by the integration of Eq. (8) by parts, to obtain

$$(10) \quad \frac{f^2}{K_1} \frac{d\theta}{dt} = \frac{\partial M_s}{\partial t} \int_0^{h_s} N \, dh - \int_0^{h_s} \left\{ \left[\int_0^h N \, dh \right] \left[\frac{\partial}{\partial h} \left(\frac{\partial M}{\partial t} \right) \right] \right\} dh$$

$$+ M_s \int_0^{h_s} \frac{\partial N}{\partial t} dh - \int_0^{h_s} \left\{ \left[\int_0^{h_s} \frac{\partial N}{\partial t} dh \right] \left[\frac{\partial}{\partial h} (M) \right] \right\} dh$$

$$+ M_s N_s \cos \xi \frac{ds}{dt}$$

where the subscripts, s, refer to the values at the satellite. Integration of the negative terms in Eq. (10) by parts puts this equation in a more straightforward form:

$$(11)\quad \frac{f^2}{K_1}\frac{d\theta}{dt} = \frac{\partial M_s}{\partial t}\int_0^{h_s} N\,dh + M_s\int_0^{h_s}\frac{\partial N}{\partial t}\,dh + M_s N_s \cos\xi\,\frac{ds}{dt}$$

$$= \left\{\left(\frac{\partial M_s}{\partial t}\int_0^{h_s} N\,dh - \int_0^{h_s}\frac{\partial M}{\partial t}\,N\,dh\right)\right.$$

$$\left. + \left(M_s\int_0^{h_s}\frac{\partial N}{\partial t}\,dh - \int_0^{h_s} M\,\frac{\partial N}{\partial t}\,dh\right)\right\} .$$

In the derivation of Eq. (10) and Eq. (11), the fact was used that $N = 0$ when $h = 0$. It is obvious that Eq. (11) could have been obtained from Eq. (8) by differentiating and adding and subtracting the proper terms.

Equation (11) is a desirable form of the first order Faraday rate of polarization rotation since the first three terms can be considered to yield approximate results with the remaining terms considered as error. The first three terms are much simpler to deal with than those of Eq. (8) and Eq. (9) because now only one function remains under the integral in the first two terms, and M_s is much easier to calculate and can be found more accurately than $\bar{M}$ since an electron distribution need not be assumed. Unfortunately the error terms are not necessarily small.

3. Second-Order Faraday Rotation

The first two terms of Eq. (1) may be differentiated to yield a second order expression for the time rate of change of the polarization plane. Performing this operation, $d\theta/dt$ is given by

$$(12)\quad \frac{d\theta}{dt} = \frac{K_1}{f^2}\left\{\int_0^S N\,\frac{\partial}{\partial t}(H\cos\phi)ds + \int_0^S H\cos\phi\,\frac{\partial N}{\partial t}\,ds + N_s H_s \cos\phi_s\,\frac{ds}{dt}\right\}$$

$$+ \frac{K_2}{f^4}\left\{\int_0^S N^2\,\frac{\partial}{\partial t}(H\cos\phi)ds + \int_0^S H\cos\phi\,\frac{\partial N^2}{\partial t}\,ds + N_s^2 H_s \cos\phi_s\,\frac{ds}{dt}\right\} .$$

It is important to examine Eq. (12), in order to show when the first order expression, Eq. (11), is a good approximation for $d\theta/dt$. All the details of this examination, however, are not presented here, and it is sufficient to note that the constant $(K_2/f^4) = 2.02 \times 10^{-13}(K_1/f^2)$ at 20 Mc is relatively small enough to negate any normal contributions

of the last three terms. On this basis, one can calculate the relative contribution of the first and fourth terms of Eq. (12) as a function of height by calculating the ratio δ which is shown in Fig. 2a where the electron distribution with height is assumed to vary as shown in Fig. 3a. The value of

$$\int N$$

is shown versus height in Fig. 2b. The relative contribution of the 4th term compared to the first term of Eq. (12) is

$$\|\text{Fourth term}\| = 2.02 \times 10^{-13}\, N_o \delta \|\text{First term}\|$$

where N_o is the maximum electron density of the ionosphere. Assuming an example for noon, $N_o = 10^{12}$ electrons/cubic meter,

$$\|\text{Fourth term}\| = (2.02 \times 10^{-13})(10^{12})(.088)\|\text{First term}\|$$

$$= .0176\ \|\text{First term}\|$$

when the signal originates 75 km above the F_2 layer maximum ($h-h_m$ = 75 km in Fig. 2a).

C. PHYSICAL PARAMETERS AND CORRECTIONS TO THE THEORY

1. Physical Quantities and Relationships

As discussed by Mitra,[24] ionized layers result from the fact that absorption of solar radiation penetrates an atmosphere in which the density increases with height. Thus the absorption decreases with depth of atmospheric penetration and a maximum point of ionization is expected. The Chapman theory[25] of layer formation is the most accepted hypothesis, and his resulting expression for the distribution of electron number density with height is given by

$$N = N_o \exp \frac{1}{2} \left\{ 1 - Z - e^{-Z} \right\} \tag{13}$$

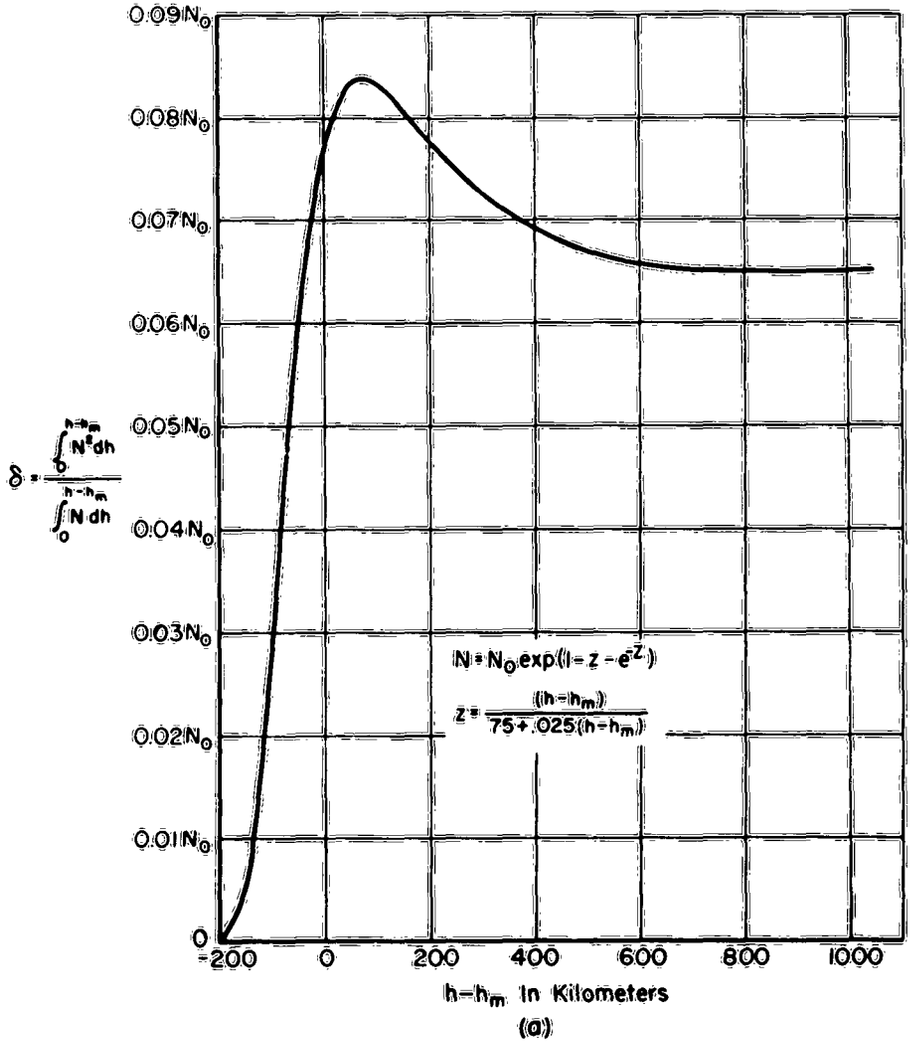

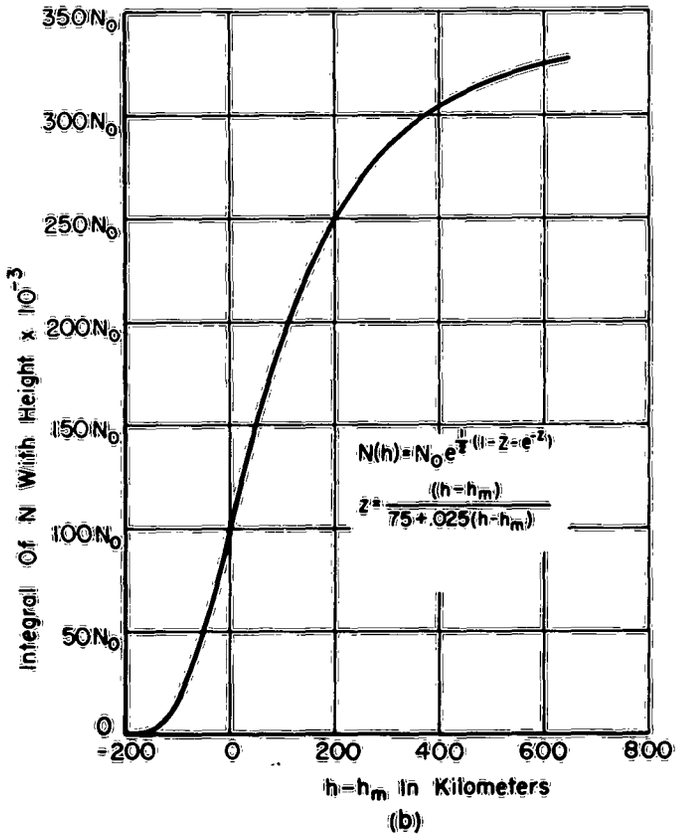

Fig. 2a. $\delta = SN^2 / SN$. Fig. 2b. Integral of electron distribution $H = 75 + \frac{5}{200}(h-h_m)$.

where

$$Z = \frac{h - h_m}{H^s}$$

h = height from the earth's surface

h_m = height of maximum ionization

N_o = maximum number density of electrons at h_m

$H^s = kT_a/mg$ = scale hieght

k = Boltzmann's constant

T_a = absolute temperature,

m = mass of electron, and

g = acceleration of gravity.

The scale height, H^s, is usually assumed to be constant in the Chapman region.

Several numbers for the scale height have been found experimentally by assuming Chapman distributions; Yeh and Swenson[8] have reported H^s=98 Km, Wright [26] has found 100 km, and Garriott[6] has found H^s = 65 km yields good agreement with experiment just above the maximum of the F_2 layer. The scale height, however, is not, in general, a constant with height, but according to recent studies,[27],[28] the ionosphere is approximately isothermal above the maximum of the F_2 layer. This means the scale height variation with altitude is inversely proportional to the acceleration of gravity, g, in the upper ionosphere. The scale height variation with time, however, is proportional to the asymptotic temperature, ergo, the intensity of the solar activity.

In previous measurements at this Laboratory,[29] it was found that the Chapman distribution and a scale height increasing linearly with height from the F_2 layer maximum at a rate of 5 km per 200 km gave good agreement with measured results of integrated electron density. This is the electron distribution which is assumed in this report where such assumptions must be made. A typical noontime variation of the electron density using this model is shown in Fig. 3a.

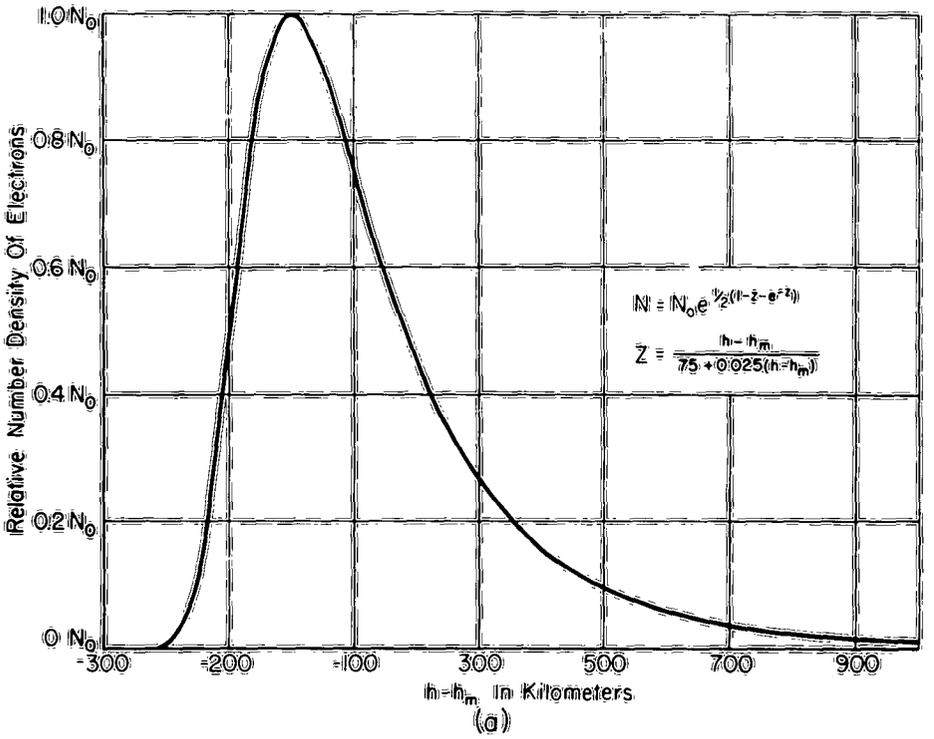

(a)

Fig. 3a. Chapman distribution.

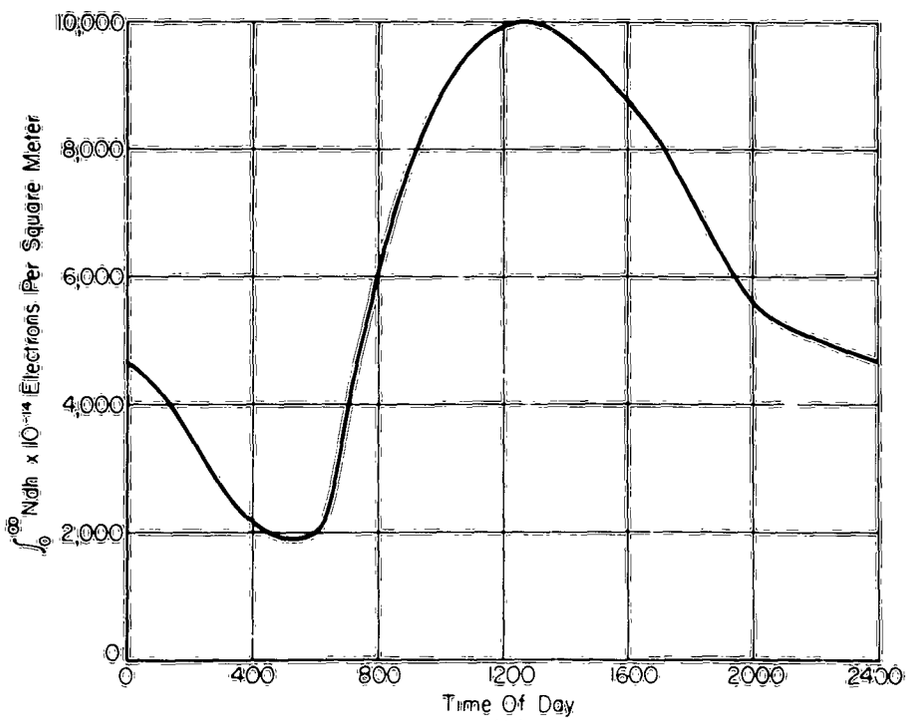

(b)

Fig. 3b. Diurnal variation.

The variation with time of N_H, as previously stated, depends on the solar activity having certain regular periods of variation: diurnal, seasonal, and sunspot-cyclical. A typical daily variation is shown in Fig. 3b which shows a two-month average on the integrated electron density to infinity, as calculated by Wright and Fine[30,31] using ionosoundings and a 100 km scale height Chapman distribution. Samples of seasonal and solar-cyclical variations may be found in Mitra.[32]

In addition to the time and height variations of electron density, horizontal gradients exist in the ionosphere. These gradients often cause serious error in experimental results[6,7] since the Explorer VII velocity relative to the earth's surface is so high that the critical frequency may change along the line of sight to the satellite by 30 to 40% in a few minutes. Under these conditions a uniform spherical stratification of the ionosphere cannot be assumed, and the integral of $\partial N/\partial t$ term in Eq. (11) may become quite large.

Now that the variation of the electron number density has been discussed, it is in order to discuss some of the other physical quantities in Eq. (11). The factor M_s, for the flat earth approximation is

$$M_s = H_s \cos \phi_s \sec \xi$$

where, to reiterate, H_s is the magnitude of the magnetic field at the satellite, ϕ_s is the angle between the magnetic-field vector and the direction of propagation at the satellite, and ξ is the angle between the direction of propagation and zenith at the satellite. Since the magnetic field is assumed to be stationary and constant at a point (see Appendix IV), and since the geometry will always be constant for a fixed observation point (see Appendix III), contours for M_s can be drawn. Figure 22 shows the value of M_s for three different satellite heights as a function azimuth and vertical angle from Columbus, Ohio.

On inspection of Fig. 22 it is obvious that the time rate of change of M_s as a satellite passes over the observation station is, for a fixed velocity, a function of the direction of travel and the nearness of approach. An infinite variety of M_s-versus-time curves is, of course, possible. Three typical Explorer VII passes are shown in Fig. 4 and the geometries are shown in Fig. 5.

The rate of change of the path length ds/dt, for this report is assumed to be the change in the optical path length or the time rate of change of the actual range. This assumption is valid if refraction and path-splitting may be neglected; this usually holds for geometries where the zenith angle is small, as shown by Garriott.[6] This time rate of change of range, or radial velocity, is always negative on the

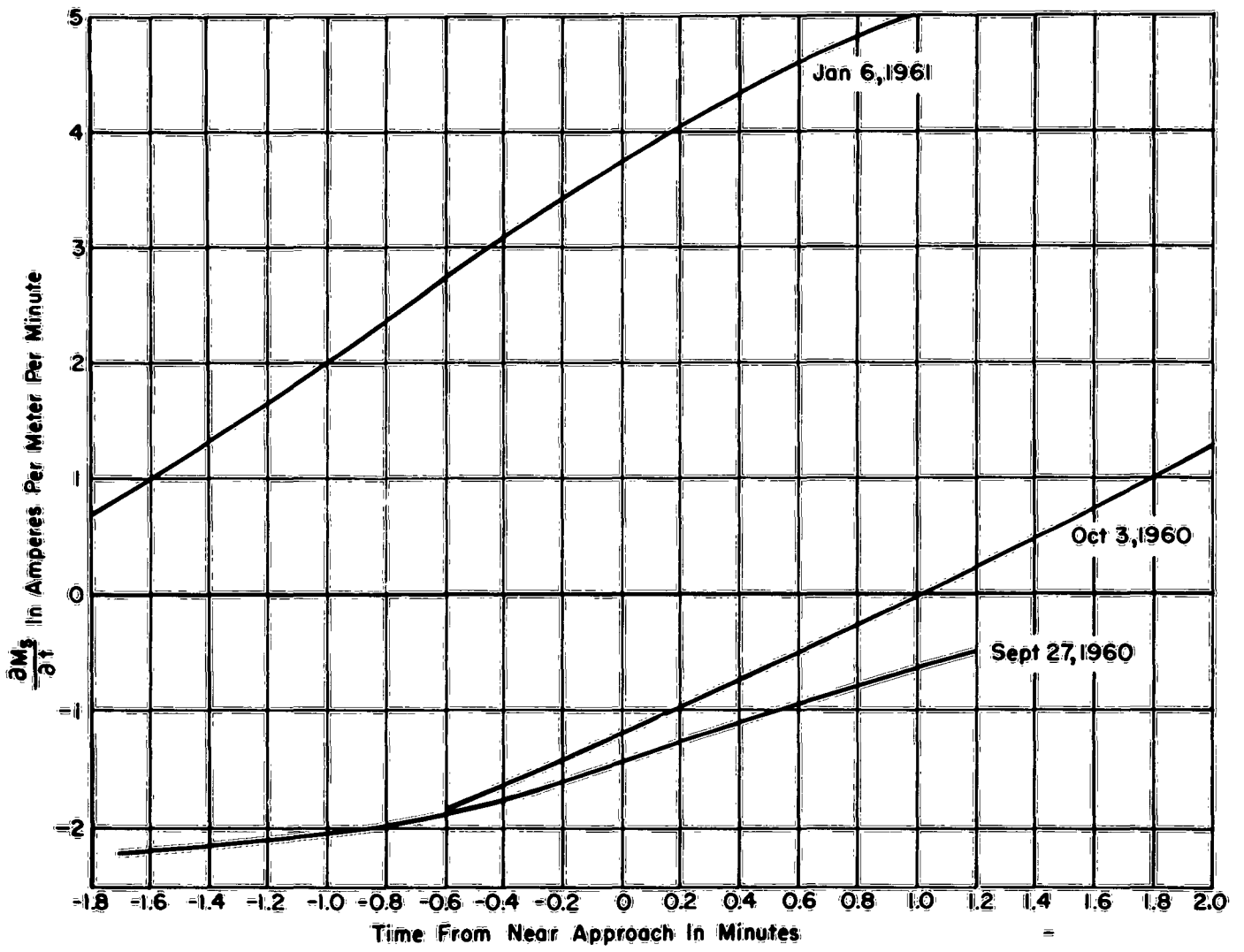

Fig. 4. 3 $\partial M_s/\partial t$ curves.

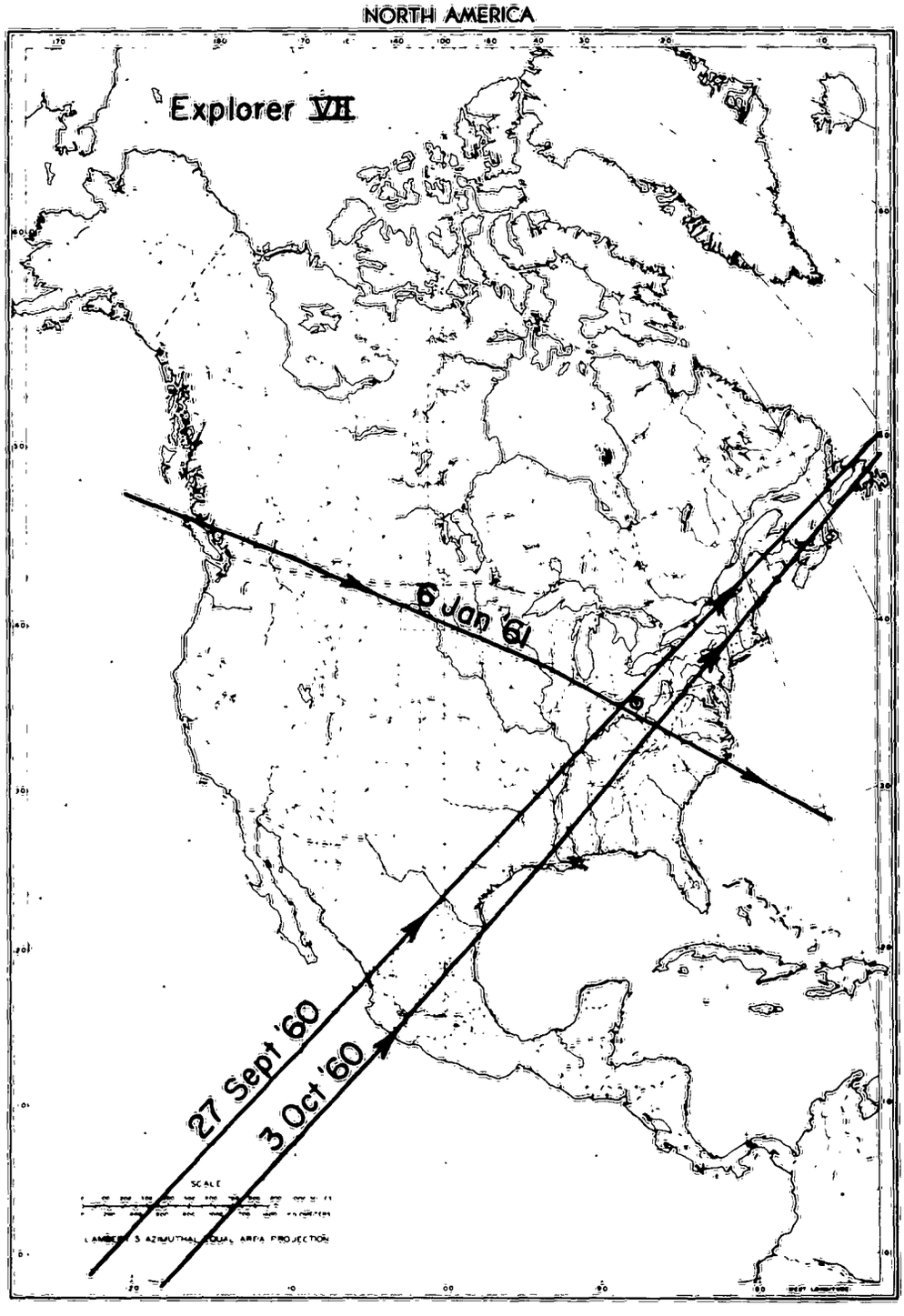

Fig. 5. Geometries for Fig. 4.

approach of the satellite, zero at the closest point of approach, and positive as the satellite moves away. A typical dr/dt curve is shown in Fig. 6.

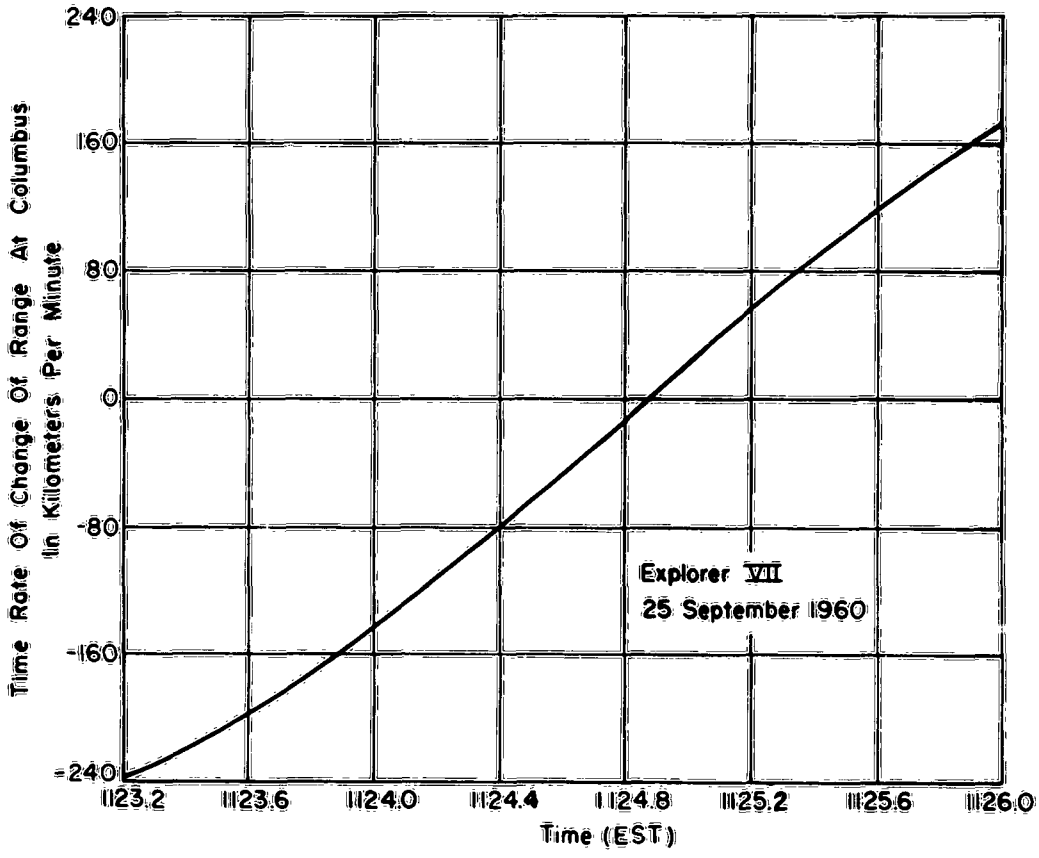

Fig. 6. dr/dt curve.

The physical quantities in Eq. (11) indicate clearly that if the "error terms" are negligible this leaves only the first three terms. But, at some point on each satellite pass $ds/dt = 0$, so that at this point Eq. (11) reduces to two terms. Furthermore, if the horizontal gradients are low the second term can be neglected and we arrive at a very simple equation:

$$(14) \quad \frac{f^2}{K_1} \frac{d\theta}{dt} = \frac{\partial M_s}{\partial t} \int_0^{h_s} N \, dh.$$

Equation (14) will be examined later in the light of experimental results to check its validity.

2. Corrections and Discussion of the Theory

Equation (2) was derived assuming that the higher order terms in Eq. (1) could be neglected. Garriott,[6] however, has outlined a procedure which compensates for this high-frequency assumption while still allowing use of the first order theory of Eq. (2). This procedure is simply to assume a model for the electron distribution with height, and then calculate the error caused by using only one term. The correction factor is then defined

$$(15) \quad \gamma = \frac{\frac{K_1}{f^2}\int_0^S NH \cos\phi \, ds}{\frac{K_1}{f^2}\int_0^S NH \cos\phi \, ds + \frac{K_2}{f^4}\int_0^S N^2 H \cos\phi \, ds + \cdots}$$

where for our case

$$N = N_o e^{\frac{1}{2}(1-z-e^z)},$$

$$z = \frac{h - h_m}{H^s},$$

$H^s = 75 + .025(h-h_m)$, the assumed scale height,

$$X_o = \frac{80.6\, N_o}{f^2} = \frac{f_c^2}{f^2}$$

N_o = the electron density at h_m, and

H = magnetic field as given in Appendix IV.

Here, X_o is a convenient parameter which adapts the calculation of γ to arbitrary frequencies. The calculated correction value for γ versus height was computed using the first five terms of the binomial expansion for θ. The results for several values of X_o are shown in Fig. 7. Using Fig. 7 and ionosonde data,[33] it is possible to find the correction for neglecting higher order terms, and a more correct form of Eq. (2) becomes

$$(16) \quad \theta = \frac{K_1}{\gamma \cdot f^2}\int_0^S NH \cos\phi \, ds$$

where γ is correct only for vertical propagation paths.

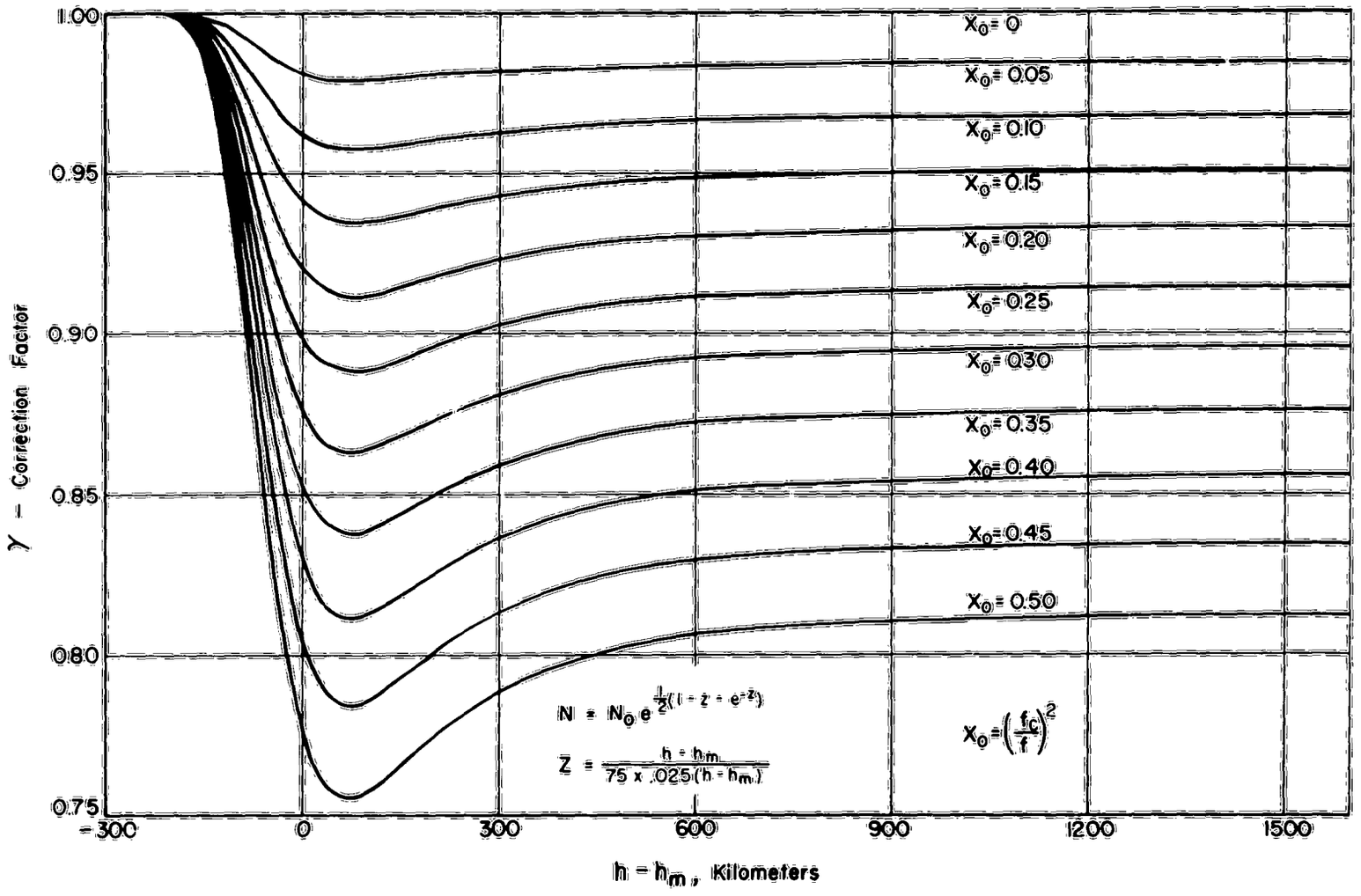

Fig. 7. Y curves.

11116-16

Starting with Eq. (16), Eq. (11) can now be written

$$(17)\quad \frac{f^2}{K_1} \cdot \gamma \cdot \frac{d\theta}{dt} = \frac{\partial M_s}{\partial t}\int_0^{h_s} N\,dh + M_s\int_0^{h_s}\frac{\partial N}{\partial t}\,dh + M_s N_s \cos\xi\,\frac{ds}{dt}$$

$$= \left\{\left(\frac{\partial M_s}{\partial t} - \overline{\frac{\partial M}{\partial t}}\right)\int N\,dh + (M_s - \overline{\overline{M}})\int\frac{\partial N}{\partial t}\,dh\right\}$$

where from the instantaneous application of the mean value theorem, when N(h) is assumed, the following are defined

$$\overline{\frac{\partial M}{\partial t}} = \frac{\int_0^{h_s} N\,\frac{\partial M}{\partial t}\,dh}{\int_0^{h_s} N\,dh}$$

and

$$\overline{\overline{M}} = \frac{\int_0^{h_s} M\,\frac{\partial N}{\partial t}\,dh}{\int_0^{h_s} N\,dh}\,.$$

Obviously, if it can be shown that

$$\frac{\partial M_s}{\partial t} \simeq \overline{\frac{\partial M}{\partial t}}$$

and

$$M_s \simeq \overline{\overline{M}}$$

then the bracketed negative error terms in Eq. (17) could be neglected. However for our initial purpose of obtaining improved values for N_H, spherical stratification is assumed as well as homogeneous layers; therefore, under this assumption N_H is assumed constant, so

$$\int_0^{h_s}\frac{\partial N}{\partial t}\,dh = 0$$

which eliminates two terms from Eq. (17), and yields at the point where $ds/dt = 0$

$$(18) \quad \frac{f^2}{K_1} \cdot Y \cdot \frac{d\theta}{dt} = \frac{\overline{\partial M}}{\partial t} \int_0^{h_s} N\,dh = \frac{\partial M_s}{\partial t} \int_0^{h_s} N\,dh - \left(\frac{\partial M_s}{\partial t} - \frac{\overline{\partial M}}{\partial t}\right) \int_0^{h_s} N\,dh.$$

As previously discussed, $\overline{\partial M}/\partial t$, is found from assuming N(h) and integrating the product MN to the satellite height at any instant. This procedure is long and N(h) must be assumed thus if the negative term in (18) can be neglected we can avoid this procedure.

For a typical Explorer VII near pass, the error term of Eq. (18) is plotted as a percentage of the first term and as a function of height in Fig. 8. In this calculation, the electron density distribution was

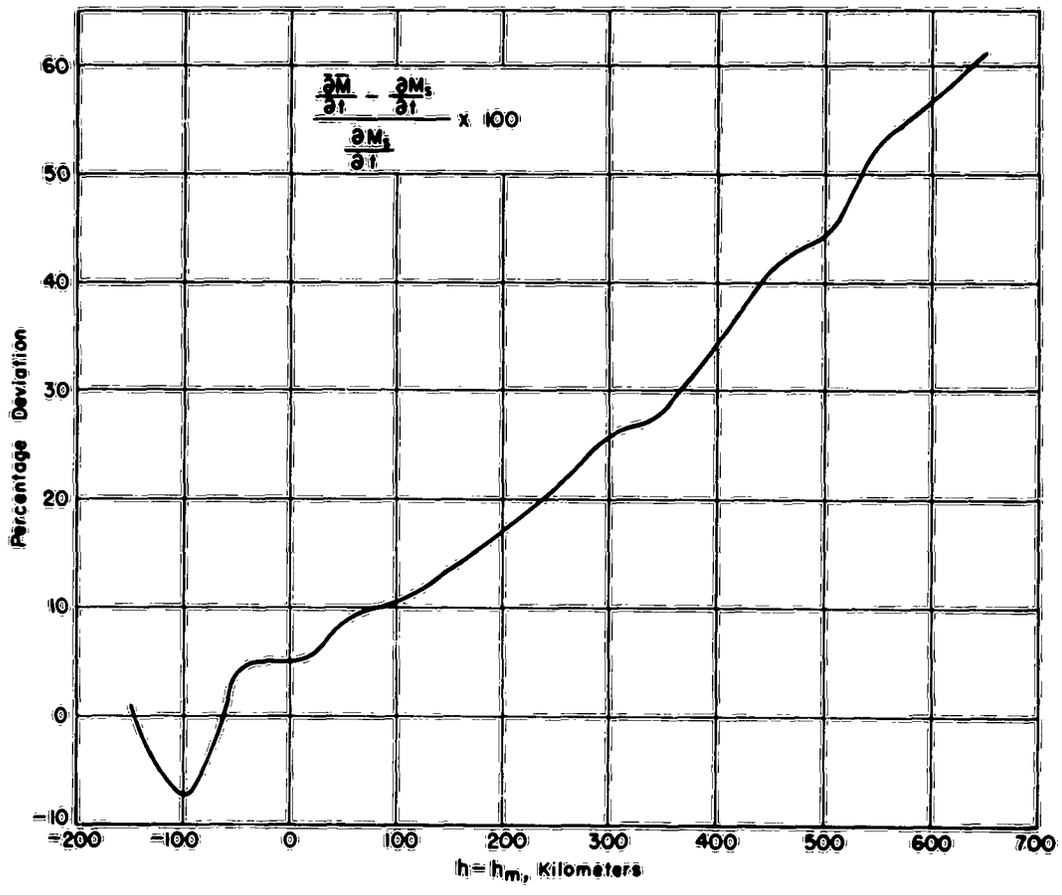

Fig. 8. $\partial M_s/\partial t$ vs $\partial \overline{M}/\partial t$.

chosen as discussed previously: a Chapman distribution with a scale height of 75 km below h_m and a scale-height gradient of +.025 above the maximum. It is seen in Fig. 8 that for typical Explorer VII heights (600 to 1100 km) the error term is much too large to neglect. It is necessary, therefore, at these heights to choose an electron distribution in order to evaluate $\partial\overline{M}/\partial t$. This procedure introduces an inherent error since the assumed N(h) will probably not have the same form as the actual N(h). Thus, the final form of the first-order equation relating the integrated electron density and the time rate of change of the polarization plane at the point of nearest approach and at low zenith angles is

$$(19) \quad N_H = \int_0^{h_s} N\,dh = \frac{\pi \cdot f^2 \cdot \gamma}{K_1 \cdot \partial\overline{M}/\partial t \cdot T}$$

where T is found experimentally and is defined in terms of the rate of change of polarization rotation as

$$T = \frac{\pi}{d\theta/dt} \quad .$$

3. <u>The Two-Point High Pass Approximation</u>

Equation (19) will yield a number for N_H which is subject to errors due to small irregularities in the ionosphere. This is an advantage if these irregularities are of interest, but the instantaneous value for N_H may be sharply affected. Therefore, it is often advantageous to average the data over a period of a minute. This is done as follows:

The value of θ is given at time t_1 by

$$\gamma \cdot \theta_1 = \frac{K_1}{f^2}\,\overline{M}_1\,N_H$$

at time t_2

$$\gamma \cdot \theta_2 = \frac{K_1}{f^2}\,\overline{M}_2\,N_H$$

or on taking the difference

$$(20) \quad N_H = \frac{f^2}{K_1} \cdot \gamma \cdot \frac{\theta_2 - \theta_1}{\bar{M}_2 - \bar{M}_1} = \frac{f^2}{K_1} \cdot \gamma \cdot \frac{\Delta\theta}{\Delta\bar{M}} \quad .$$

Thus by working with two points at a high altitude where N_H can be assumed to be constant with height, we have a simple expression for N_H. The data used are the number of radians change in the measured Faraday polarization rotation in the time interval $t_2 - t_1$. Here again, the data are used near the point of closest approach, avoiding vertical angles of greater than 40° from zenith so as to minimize errors due to path-splitting and refraction.

D. EXPERIMENTAL RESULTS

1. Integrated Electron Density to the Satellite

Figure 9 shows a logarithmic recording of the regular Faraday fades due to the polarization rotation of the Explorer VII satellite as received by two orthogonal dipoles (see Appendix VI) at a frequency of 19.9904 Mc. The period between each null is, T, corresponding to the time elapsed for a change of π radians in the polarization plane at a particular linear antenna. These values of T represent the experimental data, and they may be found as a function of time as shown in Fig. 10.

Using the values of T at near approach for 28 overhead passes of 1959 Iota I, the integrated electron density, N_H, was found by Eq. (19). The results are shown in Fig. 11 along with the value of SH_{max} at Fort Monmouth, New Jersey. SH_{max} is the integrated electron density to the maximum of the F_2 layer. Fort Monmouth is at approximately the same latitude as Columbus, Ohio, but Fort Monmouth is at 74° W longitude while Columbus is at 83°W longitude; this roughly means that Fort Monmouth is 0.6 hours ahead of Columbus in terms of diurnal solar position. This fact must be allowed for in examining the Ft. Monmouth ionosounding data; these corrected data, however, will not generally yield the same data that would have been found at Columbus directly. The agreement in Fig. 11 however, is quite good, and, in fact, a cross-correlation of +0.86 is obtained between SH_{max} and N_H, and these data are presented again in Table I.

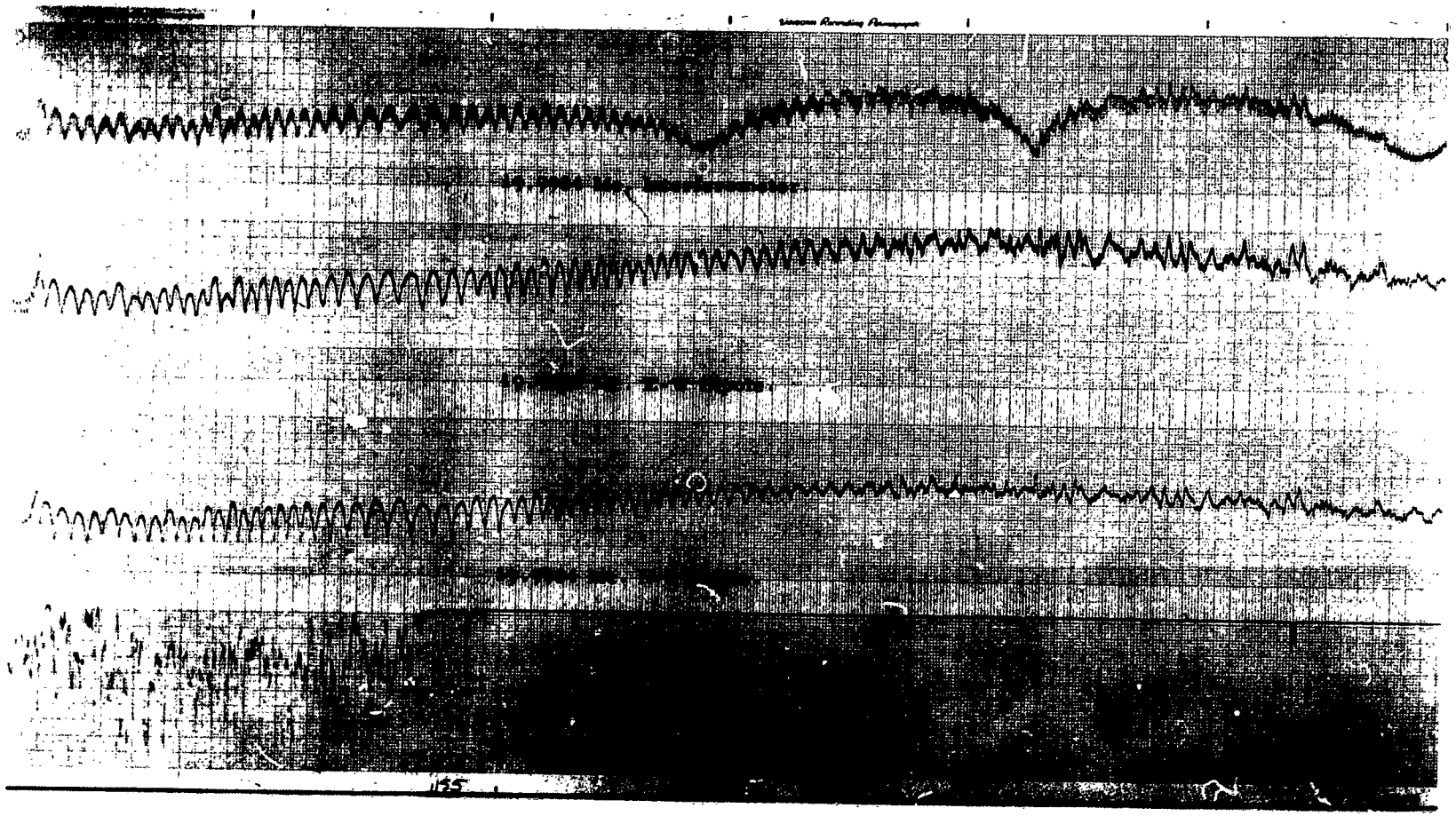

Fig. 9. Sanborn record.

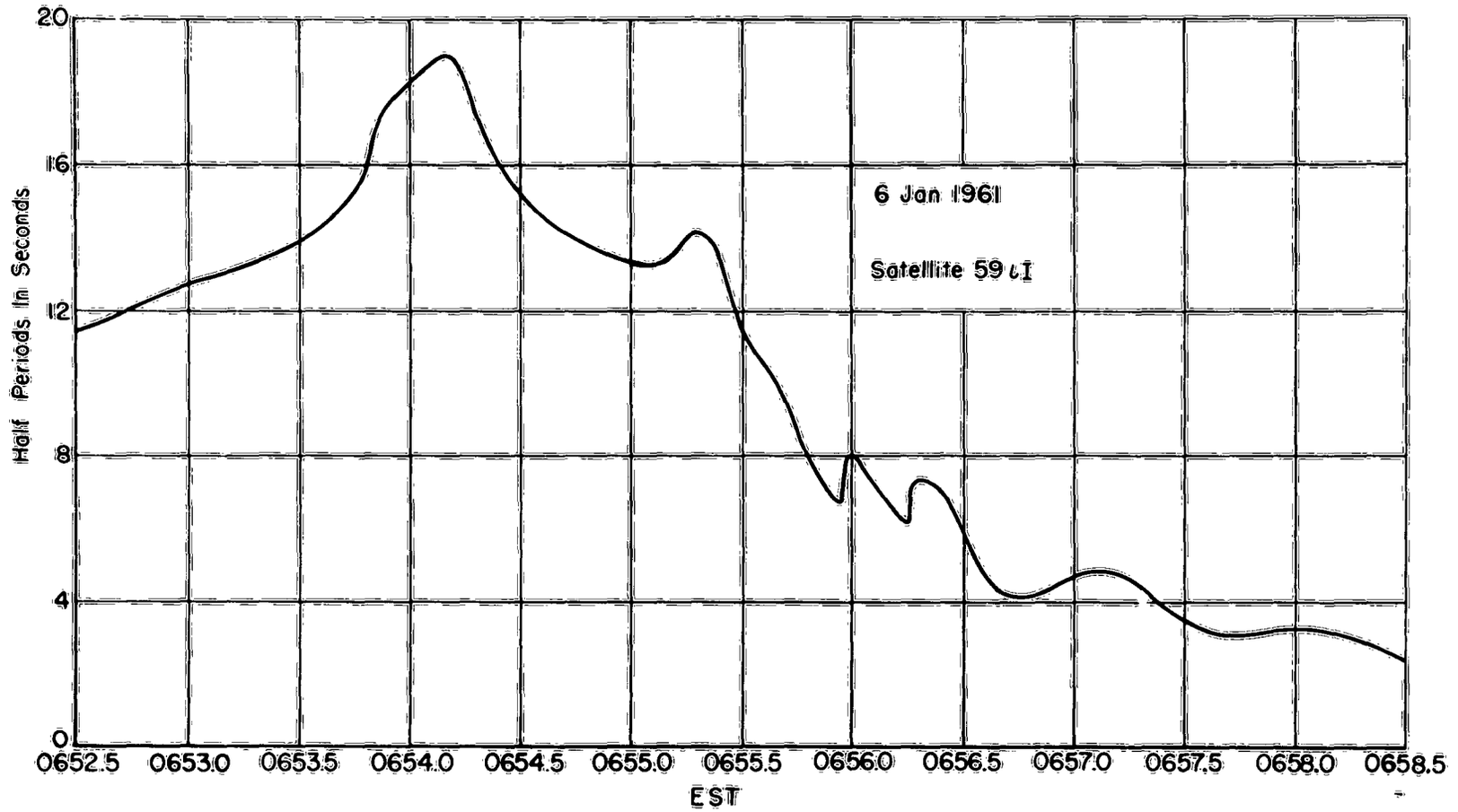
6 Jan 1961
Satellite 59 ι I
Half Periods In Seconds
20
16
12
8
4
0
0652.5
0653.0
0653.5
0654.0
0654.5
0655.0
0655.5
0656.0
0656.5
0657.0
0657.5
0658.0
0658.5
EST

Fig. 10. T vs t.

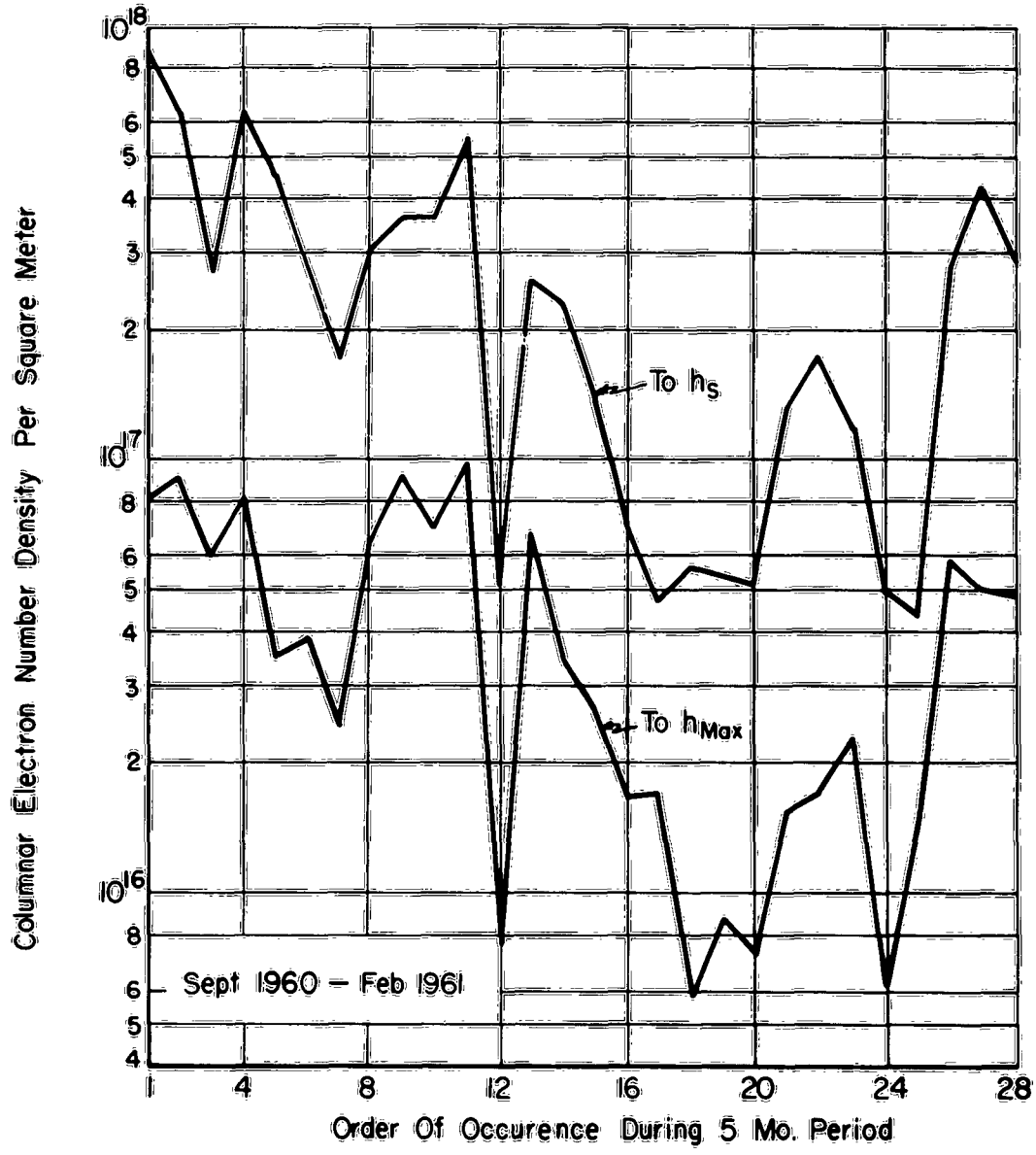

Fig. 11. N_H vs SH_{max}.

Another method of presenting the results is to show the values obtained for the columnar electron density to the satellite, N_H, and the corresponding values of the columnar electron density to the F_2 maximum, SH_{max}, as a function of the time of day of the occurrence. These plots are shown in Fig. 12. The smooth curves drawn through

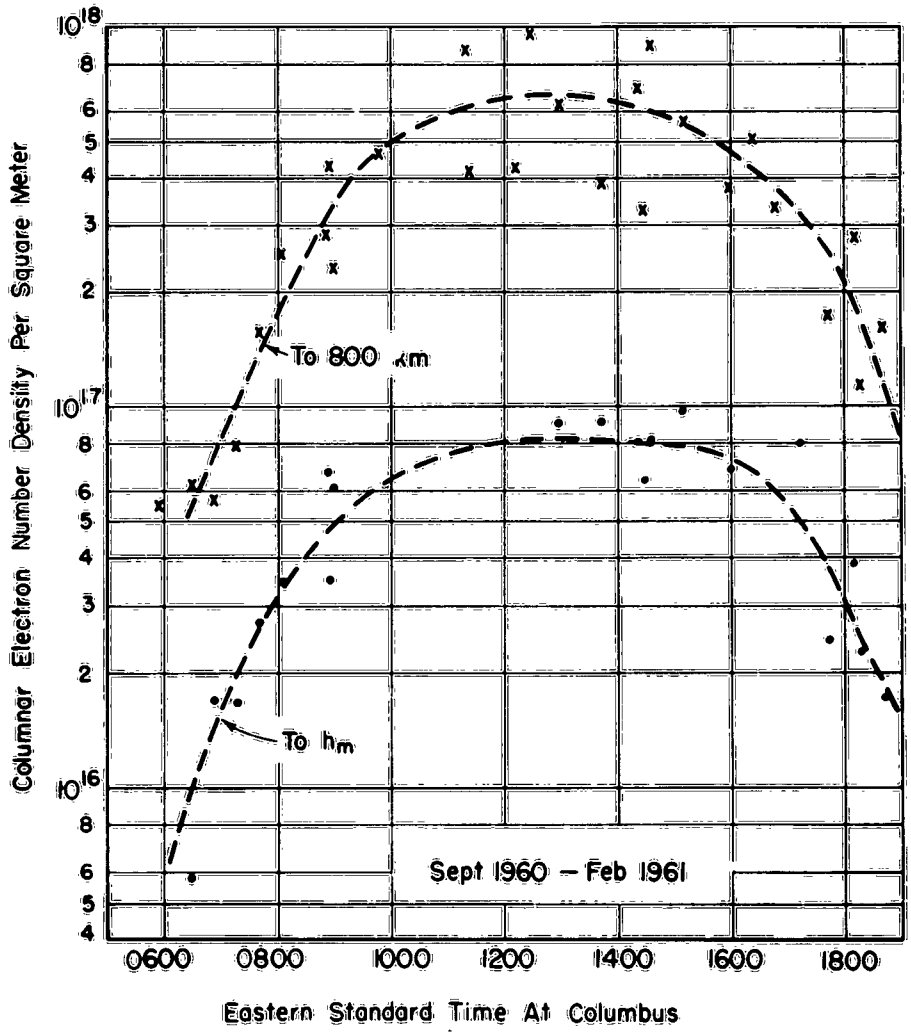

Fig. 12. N_H, SH_{max} as a function of time of day.

the results in Fig. 12 show practically an identical variation in N_H and SH_{max}. In this small sample, then, the variation of N_H as shown by Ross,[34] which has an increasing N_H in the hours 1400-1800, has not been verified. Ross[34] has hypothesized that while the ionization below the maximum decreases during these hours the total electron content, expecially above the maximum continues to build up.

2. Ionization above the F_2 Layer Maximum

Another result of interest is the ratio of the total electron content above the F_2 maximum to that below. This ratio is presented in Fig. 13

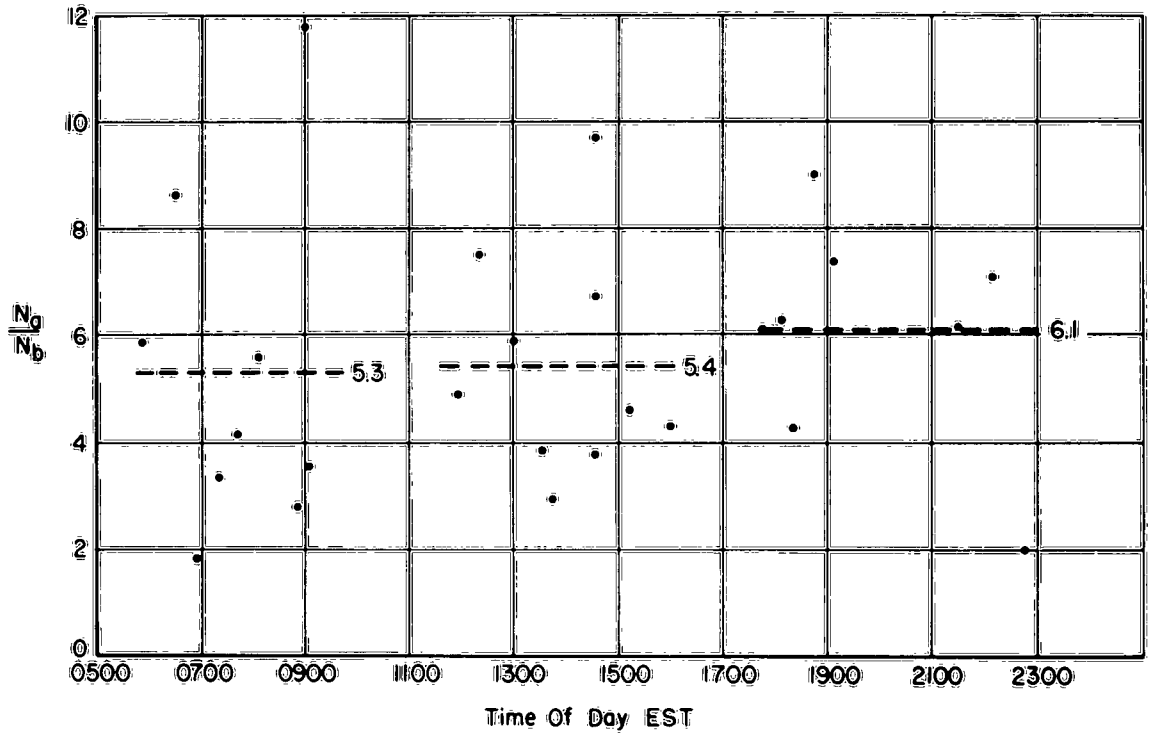

Fig. 13. N_a/N_b.

as a function of time of day of the occurrence. Figure 12 illustrates that a large percentage of the total ionization may lie above the F_2 maximum at any time of day. Figure 13 shows an average ratio of N_a/N_b of 5.3 during the morning hours, 5.4 during midday, and 6.1 during the evening. These results are slightly higher than those reported by other investigators. Evans,[35] for example, has reported, N_a/N_b = 3 or less to 4; Bauer and Daniels,[36] 3 to 5; Hill and Dyce,[37] 1.5 to 2.5; and Millman and Sanders,[38] 3 to 8. It may be noticed that four points in Fig. 13 lie above a ratio of N_a/N_b = 8.

3. Equivalent Heights of the Ionosphere

The equivalent heights, as described by Garriott,[6] were found as a method of comparison. These equivalent heights, Y, are found by taking the ratio

$$Y = \frac{N_H - SH_{max}}{N_{max}} ,$$

which yields the height of the column having a cross section of one square meter and a uniform electron density N_{max}, but which contains a total number density of electrons that is equal to $N_H - SH_{max}$. These equivalent heights are shown in Fig. 14 as a function of $h_s - h_{max}$, the height of the satellite above the F_2 maximum. Figure 14 shows an average equivalent height of 305 km for the 28 near passes analyzed. The theoretical value of the asymptotic equivalent height is 217 km based on the assumed Chapman distribution and the assumed variation of scale height. The values obtained for the equivalent heights, Y, found here are approximately 75% higher than those found by Garriott.[6] However, magnetically disturbed days, which usually yield higher values of Y, were not eliminated from these data as they were in Garriott's work.

4. The Effect of Magnetic Disturbance on N_H

An attempt was made to correlate the values obtained for N_H with the inverse of the 24-hour average of the magnetic K index.[39] This approach followed that of Ross, but no positive correlation was shown, in fact the cross correlation had a value of -0.24. These values are also included in Table I.

It is pointed out here for clarity that while N_H, apparently, is not affected appreciably by magnetic disturbances this does not mean that N is not affected. The effect may arise at a specific range of heights as a perturbation; for example, N_{max} is shown by Garriott[6] to vary with the magnitude of the magnetic disturbance.

5. The Integrated Electron Density from Longer Periods of Observation

Using Eq. (20) the values of N_H were recalculated in order to compare the results with those obtained at near-approach by Eq. (19). This method has the advantage of integrating out horizontal irregularities

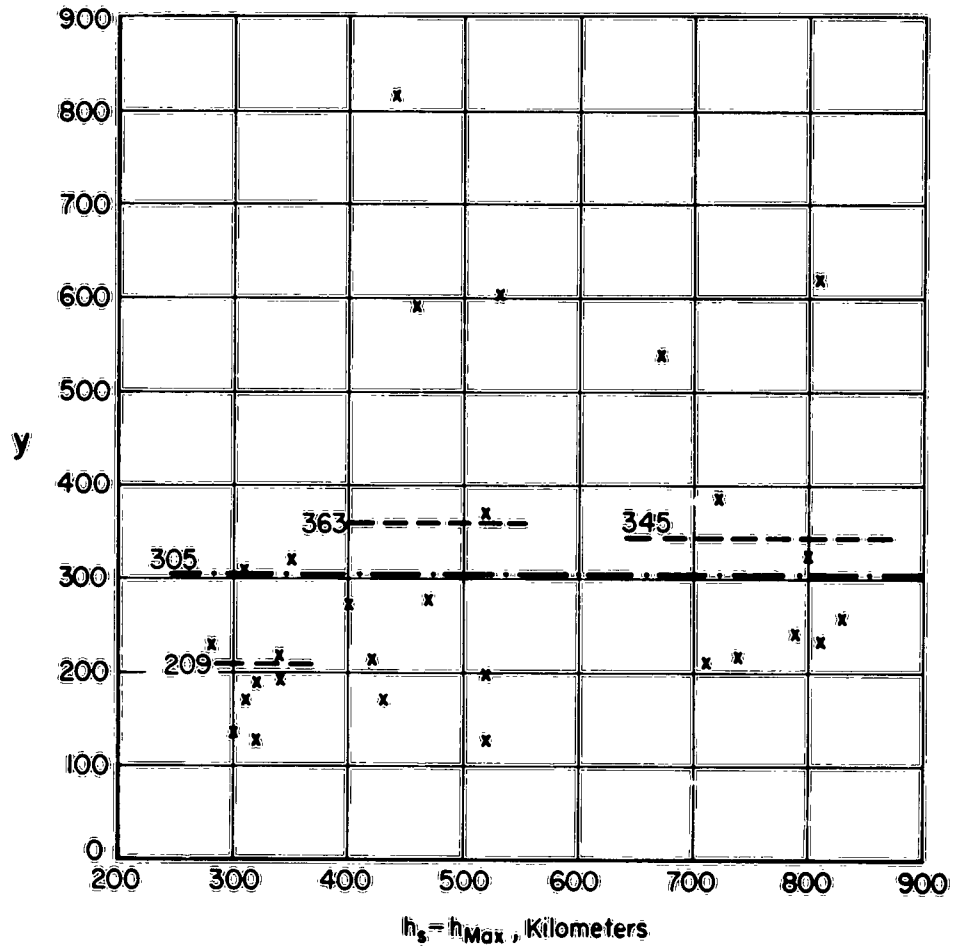

Fig. 14. N_a/N_{max}.

in the ionosphere up to 50 or 100 km in extent when an observation of one minute is used. It also has the disadvantage that errors due to local effects and path-splitting are not minimized. Also, errors in satellite position as a function of time often tend to yield erratic results.

The columnar or integrated electron density calculated using Eq. (20) is plotted in Fig. 15a as $N_H\bar{P}$. Also plotted are the instantaneous values of N_H at near approach and a theoretical value N_{TH}. The theoretical value, N_{TH}, was calculated from the ionosounding data at Fort Monmouth and is given by

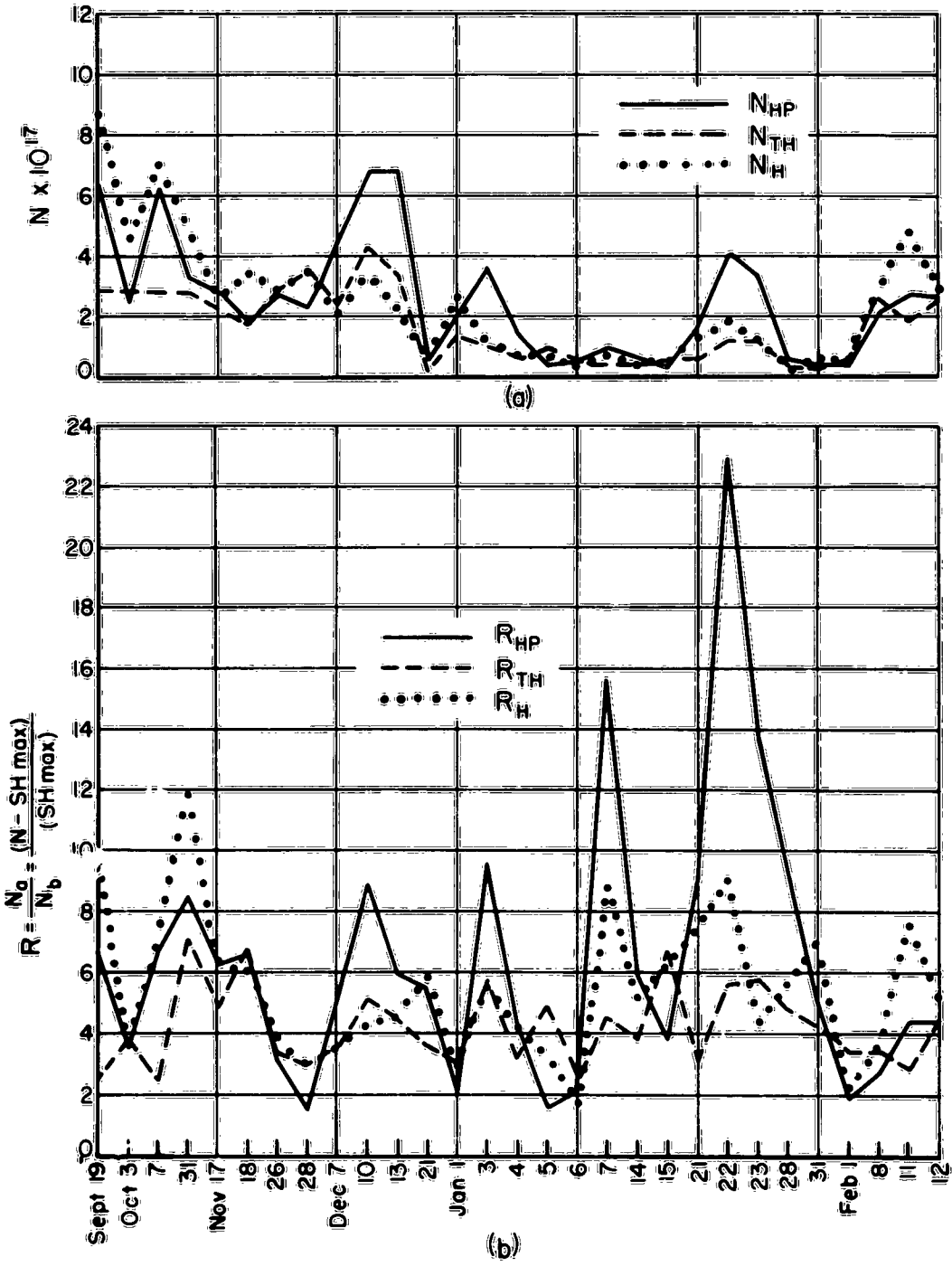

Fig. 15. High pass data (a) N_{HP} N_{TH} N_H (b) R_H R_{HP} R_{TH}.

TABLE I

TABULAR RESULTS OF NEAR PASSES OF EXPLORER VII

Date	Time	$h_s - h_m$	SH_{max}	N_{max}	$\frac{1}{\Sigma K}$	N_H	N_{HP}
19 Sept '60	1434.4±.5	440	8.13×10^{16}	953×10^{9}	.1111	87.2×10^{16}	6.28×10^{17}
23 Sept	1259.3±.4	535	9.07×10^{16}	892×10^{9}	.0526	62.8×10^{16}	=
24 Sept	1236.1±.2	530	=	765×10^{9}	=	95.5×10^{16}	6.71×10^{17}
25 Sept	1212.3±.4	560	=	=	.0909	42.9×10^{16}	5.55×10^{17}
27 Sept	1124.8±.9	600	=	=	.0400	42.3×10^{16}	3.93×10^{17}
1 Oct	0949.3±.4	710	=	=	.0313	48.0×10^{16}	4.80×10^{17}
3 Oct	0901.5±.6	740	6.02×10^{16}	980×10^{9}	.0370	27.3×10^{16}	2.62×10^{17}
7 Oct	1433.1±.2	460	8.09×10^{16}	921×10^{9}	.0189	62.6×10^{16}	6.21×10^{17}
15 Oct	1122.0±.1	600	=	=	.0769	89.9×10^{16}	10.25×10^{17}
21 Oct	0858.6±.7	720	3.50×10^{16}	1072×10^{9}	.0625	44.8×10^{16}	3.31×10^{17}
17 Nov	1810.1±.2	490	3.86×10^{16}	878×10^{9}	.0385	28.2×10^{16}	2.82×10^{17}
18 Nov	1746.0±.1	520	2.44×10^{16}	754×10^{9}	.0667	17.4×10^{16}	1.86×10^{17}
26 Nov	1433.7±.8	340	6.41×10^{16}	1119×10^{9}	.0625	30.6×10^{16}	2.66×10^{17}
28 Nov	1345.7±.8	340	9.16×10^{16}	1406×10^{9}	.0294	36.2×10^{16}	2.32×10^{17}
7 Dec	1714.1±.2	500	8.02×10^{16}	1323×10^{9}	.0476	=	16.52×10^{17}
8 Dec	1649.7±.8	420	=	=	.1250	32.6×10^{16}	6.48×10^{17}
9 Dec	1625.6±.7	410	=	=	.0625	48.8×10^{16}	5.51×10^{17}
10 Dec	1601.4±.5	430	6.83×10^{16}	1712×10^{9}	.1429	36.3×10^{16}	6.83×10^{17}
12 Dec	1513.1±.2	420	9.71×10^{16}	2092×10^{9}	.0588	54.5×10^{16}	6.82×10^{17}
22 Dec	0552.8±.9	350	$.75 \times 10^{16}$	138×10^{9}	.2000	5.16×10^{16}	$.484 \times 10^{17}$
1 Jan '61	0855.3±.4	310	6.79×10^{16}	1107×10^{9}	.0476	25.6×10^{16}	2.10×10^{17}
3 Jan	0806.6±.7	320	3.46×10^{16}	1033×10^{9}	.0769	22.8×10^{16}	3.67×10^{17}
4 Jan	0742.3±.4	280	2.70×10^{16}	489×10^{9}	.1000	13.9×10^{16}	1.432×10^{17}
5 Jan	0719.7±.8	320	1.66×10^{16}	433×10^{9}	.1250	7.18×10^{16}	4.31×10^{17}
6 Jan	0655.5±.6	300	1.70×10^{16}	227×10^{9}	.0476	4.78×10^{16}	$.520 \times 10^{17}$
7 Jan	0631.2±.3	310	$.58 \times 10^{16}$	140×10^{9}	.1667	5.61×10^{16}	$.964 \times 10^{17}$
14 Jan	0342.2±.3	400	$.88 \times 10^{16}$	165×10^{9}	.0667	5.35×10^{16}	$.6112 \times 10^{17}$
15 Jan	2133.2±.3	710	$.72 \times 10^{16}$	209×10^{9}	.1667	5.17×10^{16}	$.3448 \times 10^{17}$
21 Jan	1907.1±.2	690	1.55×10^{16}	212×10^{9}	.0313	12.99×10^{16}	1.57×10^{17}
22 Jan	1842.8±.9	800	1.71×10^{16}	415×10^{9}	.0500	17.15×10^{16}	4.11×10^{17}
23 Jan	1818.4±.5	790	2.27×10^{16}	399×10^{9}	.0526	11.98×10^{16}	3.34×10^{17}
28 Jan	2323.8±.9	500	$.63 \times 10^{16}$	139×10^{9}	.0555	=	$.561 \times 10^{17}$
31 Jan	2210.7±.8	520	$.61 \times 10^{16}$	117×10^{9}	.1111	4.94×10^{16}	$.364 \times 10^{17}$
1 Feb	2146.4±.5	520	1.48×10^{16}	228×10^{9}	.0909	4.39×10^{16}	$.431 \times 10^{17}$
8 Feb	1334.0±.1	810	5.76×10^{16}	852×10^{9}	.0715	27.89×10^{16}	2.15×10^{17}
10 Feb	1245.2±.3	790	=	=	.3333	26.77×10^{16}	1.96×10^{17}
11 Feb	1220.7±.8	810	4.96×10^{16}	603×10^{9}	.0833	42.30×10^{16}	2.69×10^{17}
12 Feb	1156.3±.4	830	4.86×10^{16}	917×10^{9}	.0833	28.67×10^{16}	2.60×10^{17}

$$N_{TH} = SH_{max} + \int_{h_{max}}^{h_s} N_{max}\, e^{\frac{1}{2}(1-z-e^{-z})}\, dh$$

where

$$z = \frac{h_s - h_{max}}{H^s}$$

and

$$H = 75 + .025\,(h_s - h_{max}) .$$

SH_{max}, N_{max} and h_{max} are derived from the ionosounding data. Figure 15a shows a maximum discrepancy on the order of a factor of three. In general, it is felt that the discrepancy between N_H and N_{TH} arises from sharp deviations in the actual scale heights from the assumed values. A method of resolving this error must be developed in any improved method of analysis. Any large discrepancy between N_H and N_{HP} arises from either small-scale irregularities or errors in the exact location of the satellite as a function of time.

Figure 15b shows the same results as shown in Fig. 15a except that the ratio of ionization above the F_2 maximum to that below is plotted; for example:

$$R_{HP} = \frac{N_{HP} - SH_{max}}{SH_{max}} .$$

The results of Fig. 15b tend to accentuate the discrepancies shown in Fig. 15a. R_{TH} and R_H agree within an order of three, but, quite surprisingly, R_{HP} tends to give larger discrepancies in comparison with R_{TH} than R_H does with R_{TH}. This tends to indicate that errors in satellite position lead to more erratic results when the observation period is longer because the large errors occur near a maximum or minimum in $\Delta M/\Delta t$ and one must work with a small difference of large numbers. The average values of the ratios are:

$$\bar{R}_{TH} = 4.16,$$

$$\bar{R}_H = 5.55, \text{ and}$$

$$\bar{R}_{HP} = 6.39.$$

6. First Order Determination of N_S

When one looks at the first-order equation for the time rate of change of the Faraday polarization rotation using the optical line of sight, r, as the propagation path, the mathematical relationship is, neglecting the term in $\partial N/\partial t$:

$$(21) \quad \frac{d\theta}{dt} \simeq \frac{K_1}{f^2}\left\{\frac{\overline{\partial M}}{\partial t} N_H + N_S M_S \cos\xi \frac{dr}{dt}\right\} .$$

Since we can only measure the magnitude

$$(22) \quad \left\|\frac{d\theta}{dt}\right\| \simeq \frac{K_1}{f^2}\left\|\frac{\overline{\partial M}}{\partial t} N_H + N_S M_S \cos\xi \frac{dr}{dt}\right\| .$$

Since in Eq. (22), N_H, N_S, M_S, and $\cos\xi$ are always positive, the sign of each term in Eq. (22) is determined by $\overline{\partial M}/\partial t$ and dr/dt. The time rate of change of range dr/dt is always negative on the approach of the satellite and positive on its departure as was shown in Fig. 6. Thus, if $\overline{\partial M}/\partial t$ is positive we can expect the magnitude of $d\theta/dt$ to become zero at some time as the satellite approaches. If $\overline{\partial M}/\partial T$ is negative the $\|d\theta/dt\|$ null will occur during the departure of the satellite. When $\overline{\partial M}/\partial t$ changes sign during the pass, the $\|d\theta/dt\|$ null position is not readily obvious and the number of nulls and the position of the nulls will depend on when $\overline{\partial M}/\partial t$ changes sign, and whether it changes from positive to negative or negative to positive.

The result of studying this $\|d\theta/dt\|$ null position is that it yields order-of-magnitude information on the ratio of N_S to N_H. In Fig. 16, three passes illustrating three different cases are shown. It is seen that if $N_S/N_H > 10^{-5}$ then the null position occurs essentially at the closest point of approach (CPA). As this ratio becomes less, however, the null can occur either considerably before the CPA, or after, depending on the sign of $\overline{\partial M}/\partial t$. Thus, under the assumptions involved, N_H/N_S may be found from the $|d\theta/dt|$ null position, and if N_H can be determined, then N_S is given directly, again, with many assumptions involved.

Figure 17 shows the agreement one obtains in using Eq. (19) to find N_H and Eq. (22) to find N_S and then comparing the theoretical computation with the experimental data. Figure 17, however, shows poor agreement. Future work incorporating path-splitting and

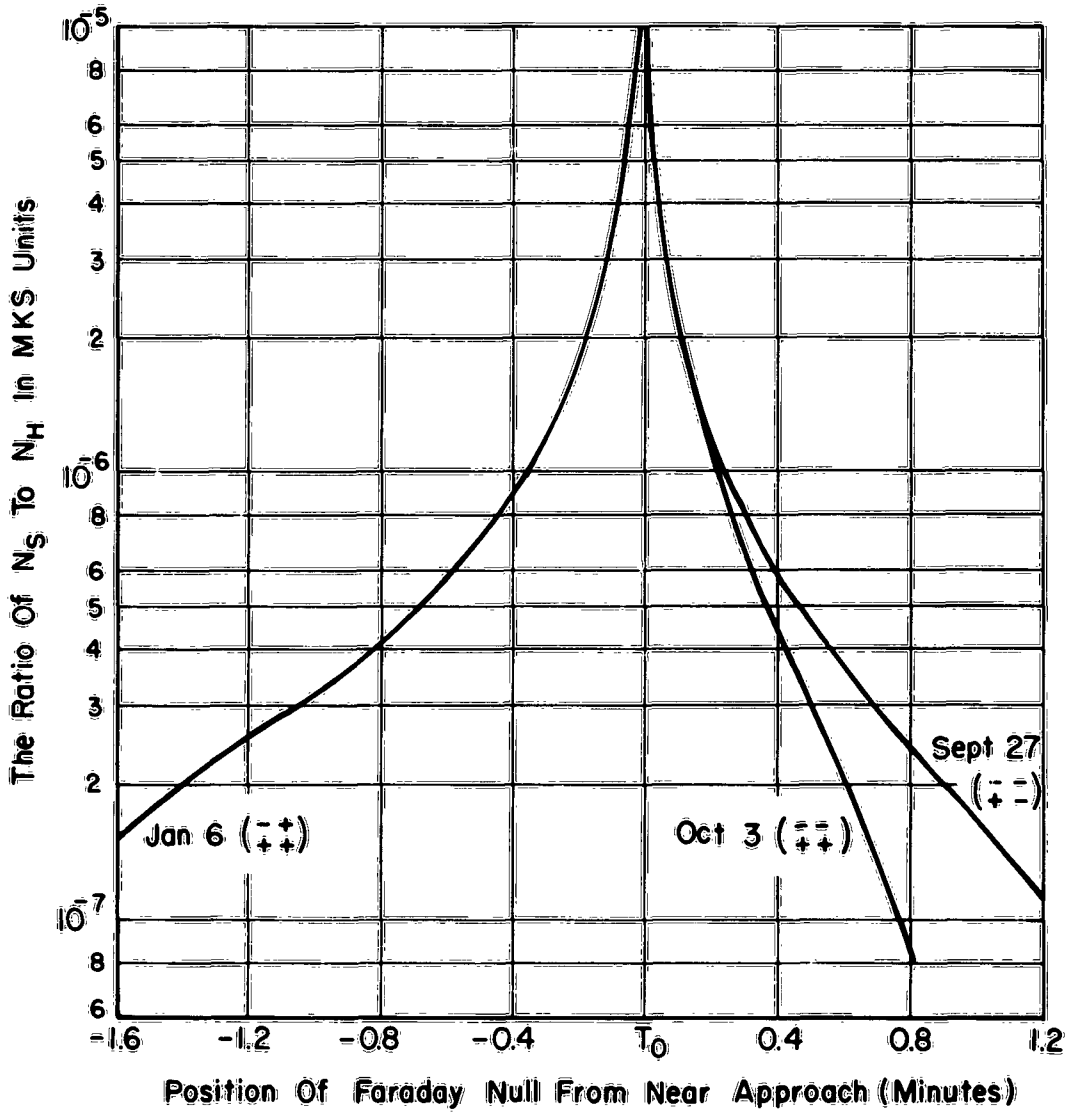

Fig. 16. T vs t, null position.

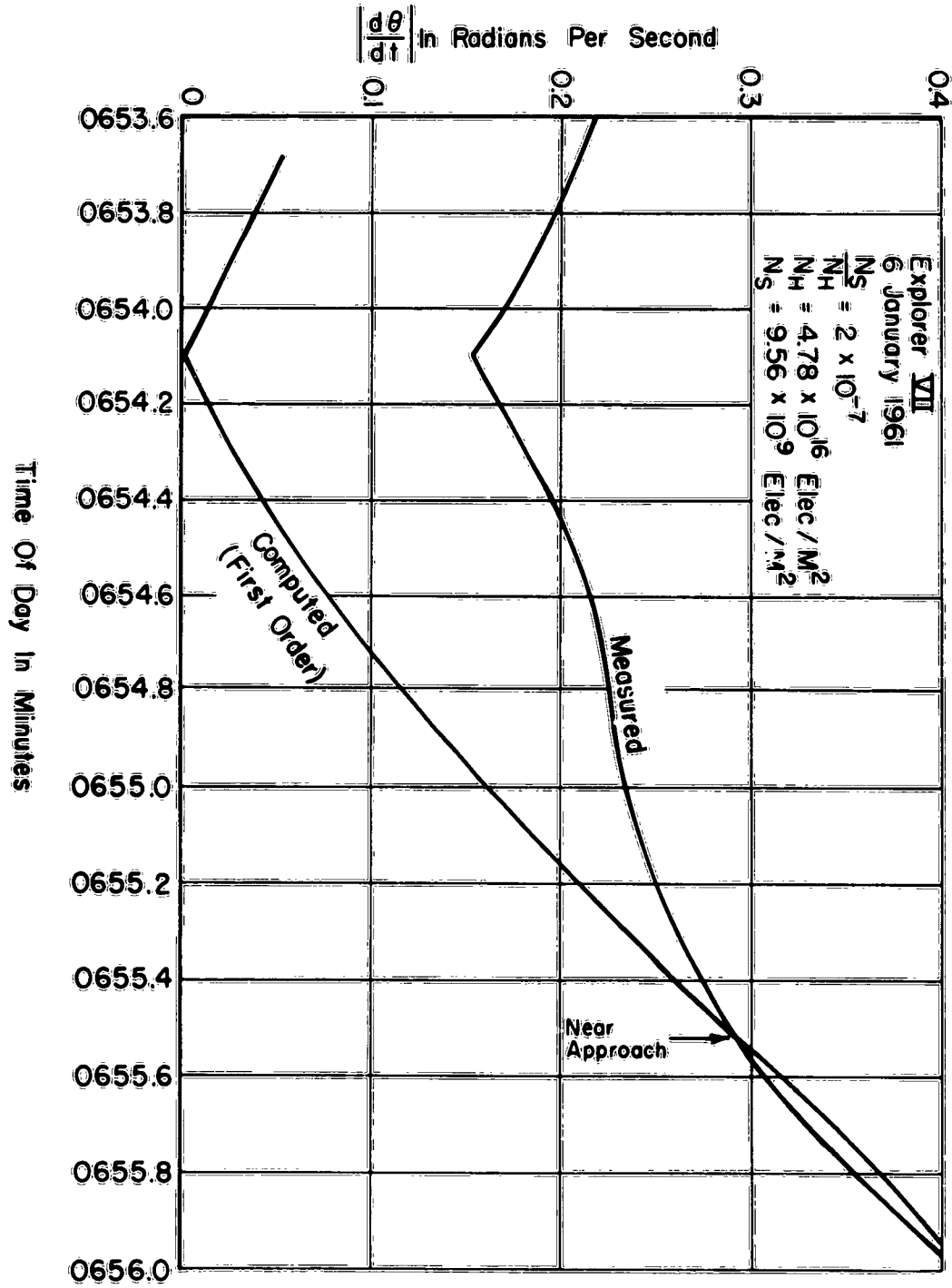

Fig. 17. Oct. 3, $|d\theta/dt|$ vs time.

refraction errors should provide much closer agreement between the experimental and theoretical curve for $\|d\theta/dt\|$ at the times away from the null point.

E. CONCLUSIONS AND RECOMMENDATIONS

Values for the integrated electron density, N_H, to the satellite may be found from single-frequency satellite signals. The accuracy of these values is improved over our previous method by (1) using an improved geomagnetic field model, (2) using the mean value of the time rate of change of the magnetic field component along the line of sight instead of the mean value of the component itself, (3) choosing only satellite passes whose near approach has a zenith angle of less than 30°, (4) evaluating N_H only at the closest point of approach of the satellite to the observation station, (5) using digital computer techniques to obtain the satellite position at small increments of time, and (6) correcting for higher order terms ignored in the analysis.

The values of N_H determined at Columbus, Ohio, correlate well, +0.86, with SH_{max}, the integrated electron density to the F_2 layer maximum determined by the National Bureau of Standards at Fort Monmouth, N.J. Also, the average values obtained for N_H, follow the average values of SH_{max} as a function of time of day and do not show a late afternoon build-up in N_H as shown by Ross.[29]

Experimental values of the electron content above the F_2 layer maximum to that below show that large ratios (N_a/N_b = 6 to 11) can occur at any time of day and not just during the evening. The average diurnal values, however, are slightly higher in the evening. The average values obtained here are generally higher than those obtained by other investigators using similar or other methods.

No correlation of the experimental values of the integrated electron densities to the satellite could be shown with magnetic disturbances.

Values of integrated electron density, N_{HP}, obtained from a longer observation period of one minute as opposed to six seconds, tended to give more erratic results. In fact, errors in the satellite position as a function of time often showed up in these values as extremely large values of N_H. The need for more accurate time corrections to satellite predictions were made obvious by this calculation.

Values for the electron density, N_S, at the height of the satellite, can be found approximately by studying the point in time where the magnitude of the time rate of change of the Faraday rotation, $\|d\theta/dt\|$, goes to zero. Ratios of $N_S/N_H > 10^{-5}$ yield a null position in $\|d\theta/dt\|$ at near approach. Lower values of this ratio retard or advance the position of the null depending on the geometry of the satellite pass. The accuracy of finding N_S depends upon the accuracy of finding N_H and accounting for variations in the ray path from the satellite to the ground as a function of the satellites position.

This report constitutes an improved look at the analysis of the Faraday effect as applied to satellite emissions. Yet, the complete analysis of these satellite signals over long periods of observation is so complicated that this report is intended only as a preliminary examination of the overall problem of obtaining electron density information in the ionosphere from the satellite signals. Specific improvements that must be made concern (1) a more accurate determination of the satellite location with time, perhaps by using interferometric techniques, (2) a better physical picture of the refracted ray paths normally encountered as a function of ionospheric conditions and the geometry of the satellite pass, (3) a correction for path-splitting of the ordinary and extraordinary rays, and (4) more diverse raw data representing various geographical locations and different satellite frequencies since these introduce new known parameters into the analysis and obviate a knowledge of the satellite antenna position.

The rate of Faraday polarization rotation of satellite signals provides a sensitive tool for studying the ionosphere, especially if the frequencies of emission lie just above the maximum critical frequency of the ionosphere. The integrated electron content, the electron density at the satellite, and the extent of ionospheric irregularities may be found conveniently from this method once the methods of analysis and types of raw data are suitably improved.

ACKNOWLEDGEMENTS

I am indebted to Mr. T. Gordon Hame for guidance in the early part of this program, and to Jean MacCluer for her help in developing computer programs and setting up many calculations. The cooperation of Dr. G.W. Swenson, University of Illinois, in providing initial geomagnetic field data is acknowledged, as well as the satellite prediction information provided by Space Track, The Smithsonian Institution, and the Goddard Space Flight Center, NASA. The Boulder Laboratories, National Bureau of Standards was of great service in providing the characteristics of the ionosphere below the F_2 layer maximum at the times of interest.

REFERENCES

1. Smith, F.G., "Ionospheric Refraction of 81.5 Mc/s Radio Waves from Radio Stars," Journal of Atmospheric and Terrestrial Physics, Vol. 2, p. 350, 1952.

2. Browne, I.C., Evans, J.V., Hargreaves, J.K., and Murray, W.A.S., "Radio Echoes from the Moon," Proceedings of the Physical Society, B, Vol. 69, p. 901, 1956.

3. Hame, T.G., and Stuart, W.D., "The Electron Content and Distribution in the Ionosphere," Proceedings of the I.R.E., Vol. 48, pp. 1786-1787, 1960.

4. Daniels, Fred B. and Bauer, Siegried J., "The Ionospheric Faraday Effect and its Applications," Journal of The Franklin Institute, Vol. 267, No. 3, March 1959, pp. 187-200.

5. Blackband, W.T., "The Determination of Ionospheric Electron Content by Observation of Faraday Fading," Journal of Geophysical Research, Vol. 65, No. 7, pp. 1987-1992, July 1960.

6. Garriott, Owen K., "The Determination of Ionospheric Electron Content and Distribution from Satellite Observations, Part I. Theory of the Analysis," Journal of Geophysical Research, Vol. 65, No. 4, pp. 1139-1150, April 1960.

7. Little, C. Gordon and Lawrence, Robert S., "The Use of Polarization Fading of Satellite Signals to Study the Electron Contents and Irregularities in the Ionosphere," Journal of Research of the National Bureau of Standards - D. Radio Propagation, Vol. 64D, No. 4, pp. 335-346, July-August 1960.

8. Yeh, K.C. and Swenson, G.W., Jr., "Ionospheric Electron Content and its Variations Deduced from Satellite Observations," Journal of Geophysical Research, Vol. 66, No. 4, pp. 1061-1068, April 1961.

9. Ross, W.J., "Integrated Electron Densities from Satellite Radio Observations," Journal of Geophysical Research, Vol. 65, No. 9, pp. 2601-2606, September 1960.

10. Kazantsev, A.N., "Absorption and Electron Distribution in the F_2 Layer Determined from Measurements of Transmitted Radio Signals from Earth Satellites," Planetary and Space Sciences, Vol. I, pp. 130-135, 17 January 1959.

11. Al'pert, Ia L., Chudesenko, E.F. and Shapiro, B.S., "Results of Research in the Outer Region of the Ionosphere from the Observations of the Radio Signals of Sputnik I," Akademiia Nauk SSSR, and Sputnikov Zernli i raket, No. 1, pp. 40-108, 1958.

12. Seddon, J.C., "Propagation Measurements in the Ionosphere with the Aid of Rockets," Rocket Exploration of the Upper Atmosphere, Pergamon Press, Ltd., London, 1954, pp. 214-222.

13. Bourdeau, R.E., "Ionospheric Results with Sounding Rockets and the Explorer VIII Satellite," International Space Science Symposium, Washington, D.C., 13 April 1961.

14. Nisbet, J.S. and Bowhill, S.A., "Electron Densities in the F Region of the Ionosphere from Rocket Measurements," Journal of Geophysical Research, Vol. 65, No. 11. pp. 3601-3614, November 1960.

15. Berning, W.N., "Earth Satellite Observations of the Ionosphere," Proceedings of the I.R.E., Vol. 47, No. 2, pp. 280-288, February 1959.

16. Evans, J.V., "The Distribution of Electrons in the Upper Ionosphere from Backscatter Observations," Report 3G-0002, Lincoln Laboratory, Massachusetts Institute of Technology, pp. 1-20, 23 November 1960.

17. Bowhill, S.A., "The Faraday-Rotation Rate of a Satellite Radio Signal," Journal of Atmospheric and Terrestrial Physics, Vol. 13, No. 1-2, pp. 175-6, December 1958.

18. Arendt, P.R., "On the Existence of a Strong Magneto-Ionic Effect Topside of the F Maximum of the Kennelly-Heaviside Layer," Jour. Applied Physics, Vol. 30, No. 5, pp. 793-795, May 1959.

19. Garriott, Owen K., "The Determination of Ionospheric Electron Content and Distribution from Satellite Observations, Part II. Theory of the Analysis," Journal of Geophysical Research, Vol. 65, No. 4, pp. 1151-1157, April 1960.

20. Hame, T.G., "Determination of the Integrated Electron Density in the Ionosphere from Earth Satellite Radio Transmission," Report 889-4, 17 March 1959, Antenna Laboratory, The Ohio State University Research Foundation, prepared under Contract AF 33(616)-6137, Air Research and Development Command, Wright Air Development Center, Wright-Patterson Air Force Base, Ohio.

21. "Techniques for Echo Area Determination - Final Engineering Report," Report 792-5, 1 February 1959, Antenna Laboratory, The Ohio State University Research Foundation; prepared under Contract AF 33(616)-5398, Air Research and Development Command, Wright Air Development Center, Wright-Patterson Air Force Base, Ohio.

22. Hame, T.G., "On Determination of the Electron Density of the Ionosphere Above N Max F_2 by Cosmic Noise Measurements," Report 1083-2, 15 July 1960, Antenna Laboratory, The Ohio State University Research Foundation; prepared under Contract AF 33(616)-7081, Air Research and Development Command, Wright Air Development Center, Wright-Patterson Air Force Base, Ohio.

23. Hame. T.G. and Stuart, W.D., "Reflection Characteristics of High Velocity Aerial Targets," Report 889-8, 16 November 1959, Antenna Laboratory, The Ohio State University Research Foundation; prepared under Contract AF 33(616)-6137, Air Research and Development Command, Wright Air Development Center, Wright-Patterson Air Force Base, Ohio.

24. Mitra, S.K., The Upper Atmosphere, The Asiatic Society, Calcutta, p. 279, 1952.

25. Chapman, S., "The Production of Ionization by Monochromatic Radiation Incident upon a Rotating Atmosphere," Proceedings of the Royal Society, Part I, Vol. 43, p. 26; Part II, Vol. 43, p. 483; 1931.

26. Wright, J.W., "A Model of the F Region Above hmax F_2," Journal of Geophysical Research, Vol. 65, No. 1, pp. 185-191, January, 1960.

27. Kallman, H.K., "Preliminary Day and Nightime Model of the Atmosphere," Presented at the Helsinki meeting, IUGG, August, 1960.

28. Nicolet, M., "The Constitution and Composition of the Upper Atmosphere," Proceedings of the IRE, Vol. 47, pp. 142-147, February 1959.

29. "Quarterly Status Report," Report 1108-1, 16 August 1960, Antenna Laboratory, The Ohio State University Research Foundation; prepared under Contract AF 19(604)-7274, Electronics Research Directorate, Air Research and Development Command, Laurence G. Hanscom Field, Bedford, Massachusetts.

30. Wright, J.W. and Fine. L.A., "Mean Electron Density Variations of the Quiet Ionosphere, March 1959," Technical Note 40-1, Boulder Laboratories, National Bureau of Standards.

31. Wright, J.W. and Fine, L.A., "Mean Electron Density Variations of the Quiet Ionosphere, April 1959," Technical Note 40-2, Boulder Laboratories, National Bureau of Standards.

32. Mitra, S.K., op. cit., 294-302.

33. "Detailed Values of Ionospheric Characteristics and F Plots," monthly publication, Central Radio Propagation Laboratory, National Bureau of Standards, Boulder, Colorado.

34. Ross, W.J., "Integrated Electron Densities from Satellite Radio Observations," Journal of Geophysical Research, Vol. 65, No. 9, pp. 2607-2615, September 1960.

35. Evans, J.V., "The Electron Content of the Ionosphere," Journal of Atmospheric and Terrestrial Physics, Vol. II, pp. 259-271, 1957.

36. Bauer, S.J. and Daniels, F.B., "Measurement of Ionospheric Electron Content by the Lunar Radio Technique," Journal of Geophysical Research, Vol. 64, No. 10, pp. 1371-1376, October, 1959.

37. Hill. R.A. and Dyce, R.B., "Some Observations of Ionospheric Faraday Rotation on 106.1 Mc/s," Journal of Geophysical Research, Vol. 65, No. 1, pp. 173-176; January, 1960.

38. Millman, G.H., Sanders, A.E., and Mather, R.A., "Radar-Lunar Investigation at a Low Geomagnetic Latitude," Journal of Geophysical Research, Vol. 65, No. 9, pp. 2619-2626; September 1960.

39. "Weekly Summary of Fredericksburg K-Indices," Weekly Publication of the Coast and Geodetic Survey, Department of Commerce.

40. Daniels, Fred B. and Bauer, Siegfried J., "The Ionospheric Faraday Effect and its Applications," Journal of the Franklin Institute, Vol. 267, No. 3, pp. 187-200, March, 1959.

41. Whitmer, R.F., "Principles of Microwave Interactions with Ionized Media," Microwave Journal, Vol. 2, No. 3, p. 50; March, 1959.

42. Jones, H.S. and Melotte, P.F., "The Harmonic Analysis of the Earth's Magnetic Field, for Epoch 1942," Monthly Notice Royal Astronomical Society, Geophysics Supplement, No. 6, p. 409, 1953.

43. Finch, H.F. and Leaton, B.R., "The Earth's Main Magnetic Field - Epoch 1955," Monthly Notice of the Royal Astronomical Society, Geophysical Supplement, No. 7, p. 314; 1957.

APPENDIX I - DERIVATION OF THE PROPAGATION CONSTANT FOR AN IONIZED MEDIUM

This Appendix follows the previous work of Hame and Stuart.[40] In the derivation, the medium is considered to be collision-free and spherically stratified with respect to the earth.

The equation of motion of a charged particle in a magnetic field and an electromagnetic field is given by Newton's second law

$$(23) \quad \bar{F} = e(\bar{E} + \bar{V} \times \bar{B}) = m \frac{\partial \bar{V}}{\partial t} \quad .$$

The force produced by the magnetic field component of the time varying electromagnetic wave, the magnetization produced by the electric field, and any polarization produced by the magnetic fields are neglected in the following discussion. The coordinate system is chosen as shown in Fig. 18 with the magnetic field lying in the Z-direction and the

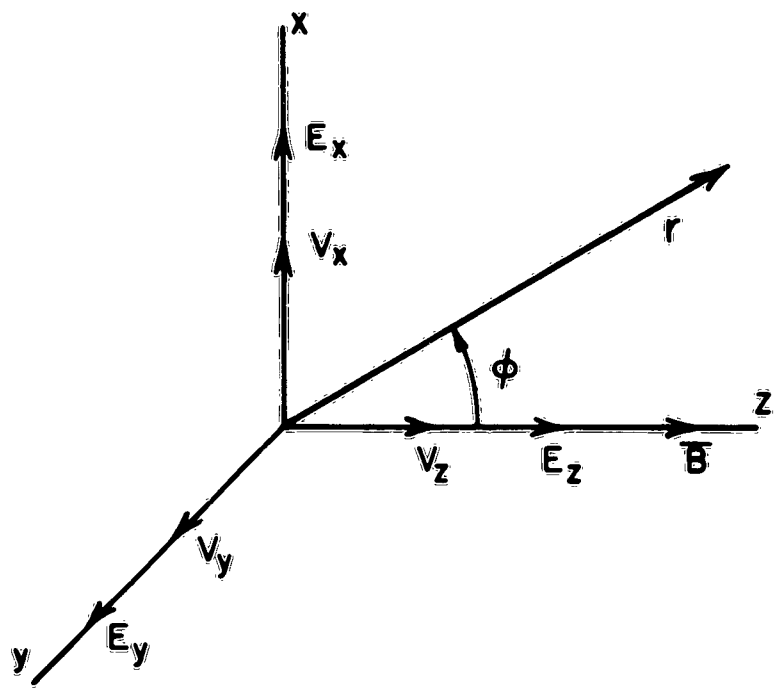

Fig. 18. Coordinates system.

direction of propagation $\bar{r}$ of the electromagnetic wave chosen to lie in the x-z plane.

On assuming that $\bar{E}$ and $\bar{V}$ are of the form $\bar{E} = E_o e_n^{j\omega t}$ and $\bar{V} = V_o e_n^{j\omega t}$, Eq. (23) becomes

$$(24)\quad \begin{cases} E_x + V_y B = \dfrac{j\omega m}{e} V_x \\[2ex] E_y - V_x B = \dfrac{j\omega m}{e} V_y \\[2ex] E_z = \dfrac{j\omega m}{e} V_z \end{cases}$$

which yields for the velocity components

$$(25)\quad \begin{cases} V_x = \dfrac{(j\omega m/e)E_x + B\,E_y}{B^2 - \left(\dfrac{m\omega}{e}\right)^2} \\[2ex] V_y = \dfrac{-B\,E_x + (j\omega m/e)E_y}{B^2 - \left(\dfrac{m\omega}{e}\right)^2} \\[2ex] V_z = \dfrac{e\,E_z}{j\omega m} \end{cases}$$

The above Eq. (25) shows that V_x and V_y become infinite as the denominator goes to zero. This angular frequency

$$(26)\quad \omega_H = \frac{e\,B}{m}$$

is the gyromagnetic frequency and this resonance occurs, for typical values of the earth's magnetic field, at $f_H = 800$ cps for hydrogen ions and at $f_H = 1.4$ mcs for electrons. Thus, at high frequencies (3-30 mcs) only the effect of electrons needs to be considered.

Maxwell's first curl equation in a region containing moving electrons may be written as

$$(27) \quad \nabla \times \bar{\bar{H}} = \epsilon_o \frac{\partial \bar{\bar{E}}}{\partial t} + Ne\bar{\bar{V}} .$$

By substituting Eqs. (25) and (26) into Eq. (27)

$$(28) \quad \nabla \times \bar{\bar{H}} = j\omega \begin{bmatrix} \epsilon_o \left\{ 1 + \frac{Ne^2}{\epsilon_o m(\omega_H^2 - \omega^2)} \right\} & \frac{-jNe^2\omega_H}{m\omega(\omega_H^2 - \omega^2)} & 0 \\ j\frac{Ne^2\omega_H}{m\omega(\omega_H^2 - \omega^2)} & \epsilon_o \left\{ 1 + \frac{Ne^2}{\epsilon_o m(\omega_H^2 - \omega^2)} \right\} & 0 \\ 0 & 0 & \epsilon_o \left(1 - \frac{Ne^2}{\epsilon_o m\omega^2} \right) \end{bmatrix} \begin{bmatrix} E_x \\ E_y \\ E_z \end{bmatrix}$$

or

$$(29) \quad \nabla \times \bar{\bar{H}} = j\omega\epsilon_{jk}\bar{\bar{E}}$$

where

$$(30) \quad e_{jk} = \begin{bmatrix} \epsilon_{11} & -j\epsilon_{12} & 0 \\ j\epsilon_{12} & \epsilon_{11} & 0 \\ 0 & 0 & \epsilon_{33} \end{bmatrix} .$$

Equation (30) defines the tensor permittivity or dielectric constant dyadic which results in the difference in direction of $\bar{E}$ and $\bar{D}$. This tensor has been presented by many authors, for example, Whitmer.[41] If the magnetic field is removed the anisotropy disappears and the tensor permittivity reduces to

$$(31) \quad \epsilon = \epsilon_o \left[1 - \frac{Ne^2}{\epsilon_o m\omega^2} \right] = \epsilon_o \left[1 - \frac{f_o^2}{f^2} \right]$$

where f_o denotes the plasma frequency.

Maxwell's second curl equation for the given time dependence is:

$$(32) \quad \nabla \times \bar{\bar{E}} = -j\omega\mu \bar{\bar{H}} \; .$$

On substituting Eq. (32) into Eq. (29) the following equation is obtained

$$(33) \quad \nabla \times \nabla \times \bar{\bar{E}} = \omega^2 \mu_o \epsilon_{jk} \bar{\bar{E}} = 0$$

where $\bar{\bar{E}}$, for our purposes, has the form

$$(34) \quad \bar{\bar{E}} = E\, e_n^{j\omega t - \bar{\bar{\gamma}} \cdot \bar{\bar{r}}}$$

and

$$\gamma = \|\bar{\bar{\gamma}}\| \, , \quad \bar{\bar{\gamma}} = \gamma \, \hat{r} \; .$$

From Fig. 18, the propagation constant γ has components

$$(35) \quad \bar{\bar{\gamma}} = \gamma_x \hat{x} + \gamma_z \hat{z} \; ; \qquad \hat{r}, \hat{x} \text{ and } \hat{z} \text{ unit vectors}$$

where

$$(36) \quad \begin{cases} \gamma_x = \gamma \sin \phi, \text{ and} \\ \gamma_z = \gamma \cos \phi \; . \end{cases}$$

Upon equating the components of Eq. (33) on the substitution of (34), (35), (36) and (30) and noticing $\partial/\partial y \; \bar{\bar{E}} = 0$ we obtain

$$(37) \quad \left(\frac{-\partial^2 E_x}{\partial z^2} + \frac{\partial^2 E_z}{\partial x \partial z} \right) \hat{x} + \left(\frac{-\partial^2 E_y}{\partial x^2} - \frac{\partial^2 E_y}{\partial z^2} \right) \hat{y} + \left(\frac{-\partial^2 E_z}{\partial x^2} + \frac{\partial^2 E_x}{\partial x \partial z} \right) \hat{z}$$

$$= \omega^2 \mu_o \epsilon_{jk} \bar{\bar{E}} = 0$$

or

$$(38)\quad \begin{bmatrix} -\gamma^2\cos^2\phi & 0 & \gamma^2\sin\phi\cos\phi \\ 0 & -\gamma^2 & 0 \\ \gamma^2\sin\phi\cos\phi & 0 & -\gamma^2\sin^2\phi \end{bmatrix} \begin{bmatrix} E_x \\ E_y \\ E_z \end{bmatrix} - \omega^2\mu_o \begin{bmatrix} \epsilon_{11} & j\epsilon_{12} & 0 \\ j\epsilon_{12} & \epsilon_{11} & 0 \\ 0 & 0 & \epsilon_{33} \end{bmatrix} \begin{bmatrix} E_x \\ E_y \\ E_z \end{bmatrix} = 0$$

on collection

$$\begin{bmatrix} -(\gamma^2\cos^2\phi + j\omega^2\mu_o\epsilon_{11}) & j\omega^2\mu_o\epsilon_{12} & \gamma^2\sin\phi\cos\phi \\ -j\omega^2\mu_o\epsilon_{12} & -(\gamma^2+\omega^2\mu_o\epsilon_{11}) & 0 \\ \gamma^2\sin\phi\cos\phi & 0 & -(\gamma^2\sin^2\phi+\omega^2\mu_o\epsilon_{33}) \end{bmatrix} \begin{bmatrix} E_x \\ E_y \\ E_z \end{bmatrix} = 0.$$

The above coefficient matrix has complex conjugate elements situated symmetrically with respect to the principal diagonal; therefore it is Hermitian. The determinant values assumed by a Hermitian form are always real, and in this case the coefficient determinant is zero.

Using the fact that the determinant is zero, γ can be solved for in terms of the other elements. The result is

$$(39)\quad \gamma^2 = -\omega^2\mu_o \left[\frac{\epsilon_{11}^2 - \epsilon_{12}^2 - \epsilon_{11}\epsilon_{33}\sin^2\phi + 2\epsilon_{11}\epsilon_{33} \mp \left\{ (\epsilon_{11}^2 - \epsilon_{12}^2 - \epsilon_{11}\epsilon_{33})^2 \sin^4\phi + 4\epsilon_{33}^2\epsilon_{12}^2\cos^2\phi \right\}^{\frac{1}{2}}}{2(\epsilon_{11} - \epsilon_{33})\sin^2\phi + 2\epsilon_{33}} \right]$$

for $\omega_H^2 \ll \omega^2$, $\epsilon_{11} \approx \epsilon_{33}$ and Eq. (39) reduces to

$$(40)\quad \gamma^2 = -\omega^2\mu_o\epsilon_{11} \left\{ 1 - \frac{\epsilon_{12}^2}{2\epsilon_{11}^2} \left[\sin^2\phi \mp \sqrt{\sin^4\phi + \frac{4\epsilon_{11}^2}{\epsilon_{12}^2}\cos^2\phi} \right] \right\}$$

which is the expression for the propagation constant of electromagnetic waves in an ionized media suiting the assumptions involved in the derivation.

APPENDIX II - DERIVATION OF THE FARADAY ROTATION EXPRESSIONS UNDER THE QUASI-LONGITUDINAL AND QUASI-TRANSVERSE CONDITIONS

1. Longitudinal and Quasi-Longitudinal Propagation

If the angle, ϕ, between the direction of propagation and the steady magnetic field is small, the propagation constant, given by Eq. (40) reduces to

$$\gamma^2 = -\omega^2 \mu_0 (\epsilon_{11} \pm \epsilon_{12} \cos \phi). \tag{41}$$

Since it is assumed that the ionosphere is lossless, the propagation constant may be replaced by the phase constant:

$$\gamma = j\beta \tag{42}$$

and

$$\beta = \omega \sqrt{\mu_0 (\epsilon_{11} \pm \epsilon_{12} \cos \phi)} \quad . \tag{43}$$

When $\phi = 0$, β represents two circularly polarized waves progressing in the r direction, as shown in Fig. 19. On assuming that the waves remain circularly polarized over the range of ϕ for which Eq. (43) applies, it is useful to develop a general expression for the change in the polarization plane per unit distance.

As illustrated in Fig. 19, $\theta_1 = \beta_1 dr$ and $\theta_2 = \beta_2 dr$, where the subscripts 1 and 2 represent the two solutions for β. The difference between the absolute angular rotations per unit distance divided by 2, i.e.,

$$d\theta = \frac{\theta_1 - \theta_2}{2} \quad , \tag{44}$$

represents the angular increment of the rotation of the plane of polarization over a distance dr. Equation (44) can also be written as

$$d\theta = \frac{\beta_1 - \beta_2}{2} \tag{45}$$

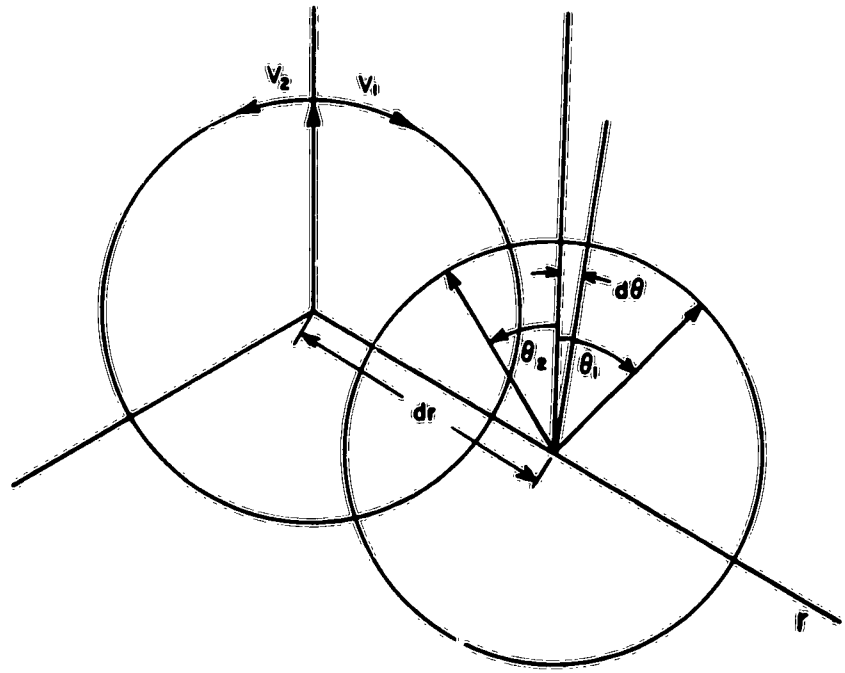

Fig. 19.

where on substitution for ϵ_{i1} and ϵ_{i2} in Eq. (43) the propagation constants are given by

$$(46) \quad \beta_{1,2} = \omega\sqrt{\mu_o \epsilon_o}\sqrt{1 - \frac{N e^2}{\epsilon_o m \omega^2}\left(1 \mp \frac{e B \cos\phi}{m\omega}\right)} \; .$$

Now letting

$$X = \frac{N e^2}{\epsilon_o m \omega^2} \qquad \text{and} \qquad Y_L = \frac{e B \cos\phi}{m\omega} \; ,$$

the expansion of β_1 and β_2 in a binomial series yields

$$(47) \quad \beta_1 = \omega\sqrt{\mu_o \epsilon_o}\left[1 - \frac{1}{2} X + \frac{1}{2} X Y_L - \frac{1}{8} X^2 + \frac{1}{4} X^2 Y_L - \frac{1}{8} X^2 Y_L^2 - \cdots\right]$$

and

$$(48) \quad \beta_2 = \omega\sqrt{\mu_o \epsilon_o}\left[1 - \frac{1}{2}X - \frac{1}{2}X Y_L - \frac{1}{8}X^2 - \frac{1}{4}X^2 Y_L - \frac{1}{8}X^2 Y_L^2 - \cdots\right].$$

From Eqs. (47) and (48),

$$(49) \quad \frac{\beta_1 - \beta_2}{2} = \frac{\omega\sqrt{\mu_o \epsilon_o}}{2}\left[X Y_L + \frac{1}{2}X^2 Y_L + \cdots\right].$$

Now on inserting the physical constants, the following equation is obtained

$$(50) \quad d\theta = \frac{\beta_1 - \beta_2}{2} = \frac{\omega\sqrt{\mu_o \epsilon_o}}{2}\left[\frac{N e^3 B \cos\phi}{\epsilon_o m^2 \omega^3} + \frac{N^2 e^5 B \cos\phi}{2\epsilon_o^2 m^2 \omega^5} + \cdots\right].$$

Now integrating Eq. (50) over a given path of length R, the total rotation of the polarization plane is

$$(51) \quad \theta = \frac{e^3}{8\pi^2 C \epsilon_o m^2 f^2}\int_0^R NB \cos\phi \, dr + \frac{e^5}{64\pi^4 C \epsilon_o^2 m^3 f^4}\int_0^R N^2 B \cos\phi \, dr + \cdots.$$

Now let

$$K_1 = \frac{e^3 \mu_o}{8\pi^2 C \epsilon_o m^2}; \qquad K_2 = \frac{e^5 \mu_o}{64\pi^4 C \epsilon_o^2 m^3}; \quad \cdots;$$

then Eq. (51) can be written

$$(52) \quad \theta = \frac{K_1}{f^2}\int_0^R NH \cos\phi \, dr + \frac{K_2}{f^4}\int_0^R N^2 H \cos\phi \, dr + \cdots.$$

Using Eq. (52) the amount of polarization rotation (Faraday effect) of an electromagnetic wave in an ionized medium can be computed where the quasi-longitudinal condition holds. The quasi-longitudinal condition holds where Eq. (41) approximates Eq. (40) to within a few percent for the propagation constant.

2. Transverse and Quasi-Transverse Propagation

If ϕ is near 90 degrees, $\cos^2\phi \approx 0$, and Eq. (40) becomes

$$(53) \quad \gamma^2 = -\omega^2 \mu_o \epsilon_{11} \left\{ 1 - \frac{\epsilon_{12}^2}{2\epsilon_{11}^2} \sin^2\phi \left[1 \mp 1 \right] \right\} .$$

The region in which this equation approximates Eq. (40) to within a few percent is known as the quasi-transverse region of propagation. In the pure transverse case, $\phi = 90^o$:

$$(54) \quad \gamma_1 = j\omega\sqrt{\mu_o \epsilon_{11}}$$

and

$$(55) \quad \gamma_2 = j\omega\sqrt{\mu_o \left(\epsilon_{11} - \frac{\epsilon_{12}^2}{\epsilon_{11}} \right)}$$

where the wave propagating with propagation constant γ_1 is known as the ordinary wave and the wave propagating with constant γ_2 is the extraordinary wave. These two waves are orthogonally oriented linearly polarized waves traveling at different velocities. This is illustrated in Fig. 20. As the waves progress from a common origin, the resultant wave becomes in sequence, elliptically, circularly, elliptically, and linearly polarized. Thus it is seen that the plane of polarization can rotate for the transverse case.

A measure of the amount of rotation that can occur under the quasi-transverse condition can be obtained following Bauer and Daniels.[4] If the two components are assumed to be circularly polarized, then from Eq. (53)

$$(56) \quad \beta = \frac{\omega}{C} \left\{ 1 - \frac{Ne^2}{2\epsilon_o m\omega^2} - \frac{\epsilon_{12}^2}{4\epsilon_o \epsilon_{11}} \sin^2\phi \left[1 \mp 1 \right] \right\}^{\frac{1}{2}} .$$

Expand Eq. (56) by the binomial expansion and taking the difference between β_1 and β_2

$$(57) \quad d\theta_t = \frac{\beta_1 - \beta_2}{2} = \frac{N e^4 B^2 \sin^2\phi}{4 C m^3 \epsilon_o \omega^3} \, dr$$

where the frequency is considered high enough to neglect the higher-order terms in the expansion. Thus, the polarization rotation in the quasi-transverse case is given by

$$(58) \quad \theta \simeq \frac{e^4}{4 C \epsilon_o m^3 \omega^3} \int_0^R N B^2 \sin^2 \phi \, dr \; .$$

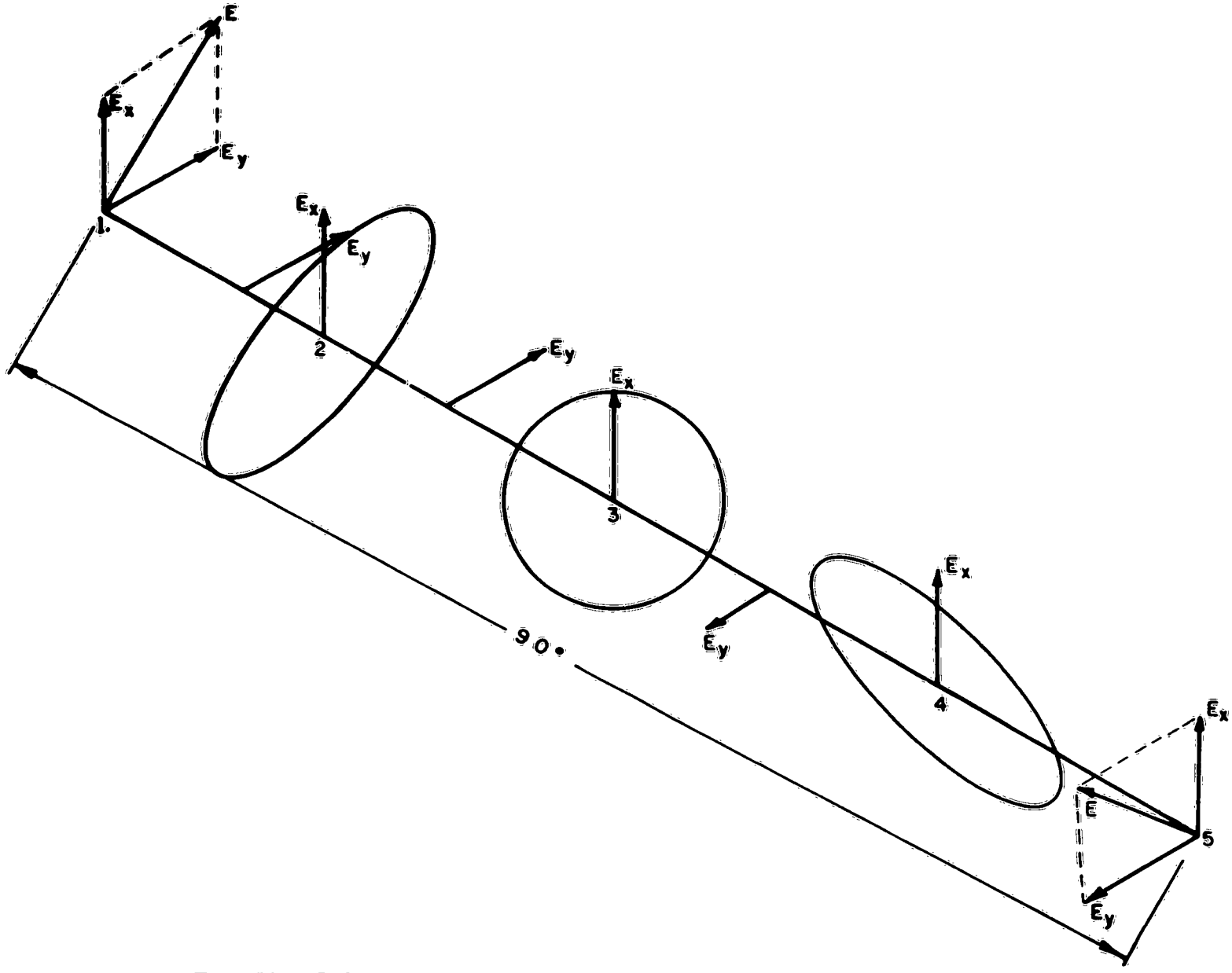

Fig. 20. Polarization rotation in the transverse case.

APPENDIX III - GEOMETRY OF A SATELLITE PASS

A problem, which arises from predictions of satellite position, is the conversion of satellite latitude, longitude, and height to azimuth, zenith angle, and range at the observing station. The definitions apply:

ϕ_1 = East longitude of the satellite,

ϕ_2 = North latitude of the satellite,

θ_1 = East longitude of the observation point,

θ_2 = North latitude of the observation point, and

a = radius of the earth = 6371 kilometers,

ψ = central angle between earth radial lines through satellite and the observation point (see Fig. 1).

The following convenient quantities are defined:

$$T_1 = \cot\left(\frac{\phi_1 - \theta_1}{2}\right) ,$$

$$T_2 = \left|\frac{\theta_2 - \phi_2}{2}\right| ,$$

$$T_3 = \left|\frac{\theta_2 + \phi_2}{2}\right| ,$$

$$T_4 = \frac{h_s}{h_s + 2a} \tan\left(\frac{\pi}{2} - \psi\right)$$

$$A = \arctan\left(\frac{T_1 \sin T_2}{\cos T_3}\right) ,$$

$$B = \arctan\left(\frac{T_1 \cos T_2}{\sin T_3}\right) , \text{ and}$$

$$C = \frac{\cos T_3 \sin B}{T_1 \cos A \cos T_2} \quad .$$

Using the above quantities, the central angle is given by

$$(59) \quad \psi = 2 \arctan C;$$

the vertical angle (or zenith angle at the observation point, see Fig. 1) is given by

$$(60) \quad i = \frac{\pi}{2} + \psi - \arctan T_4;$$

and, the range is given by

$$(61) \quad r = \frac{(h_s + a) \sin(\psi)}{\sin i} \quad .$$

Using Eqs. (2) and (3), Fig. 21 shows the azimuth and vertical angle curves for three satellite heights at Columbus, Ohio.

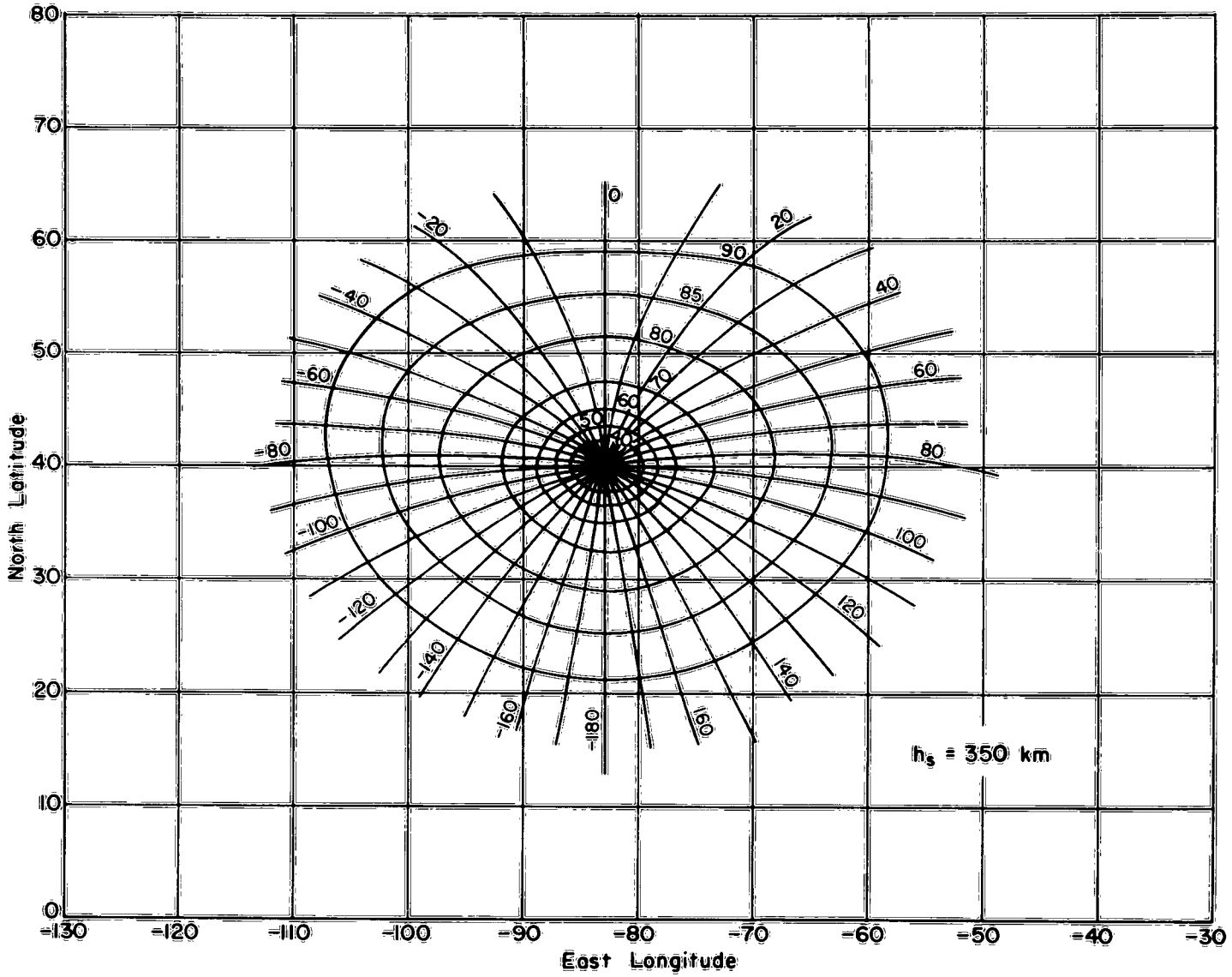

Fig. 21a. az-Va 350.

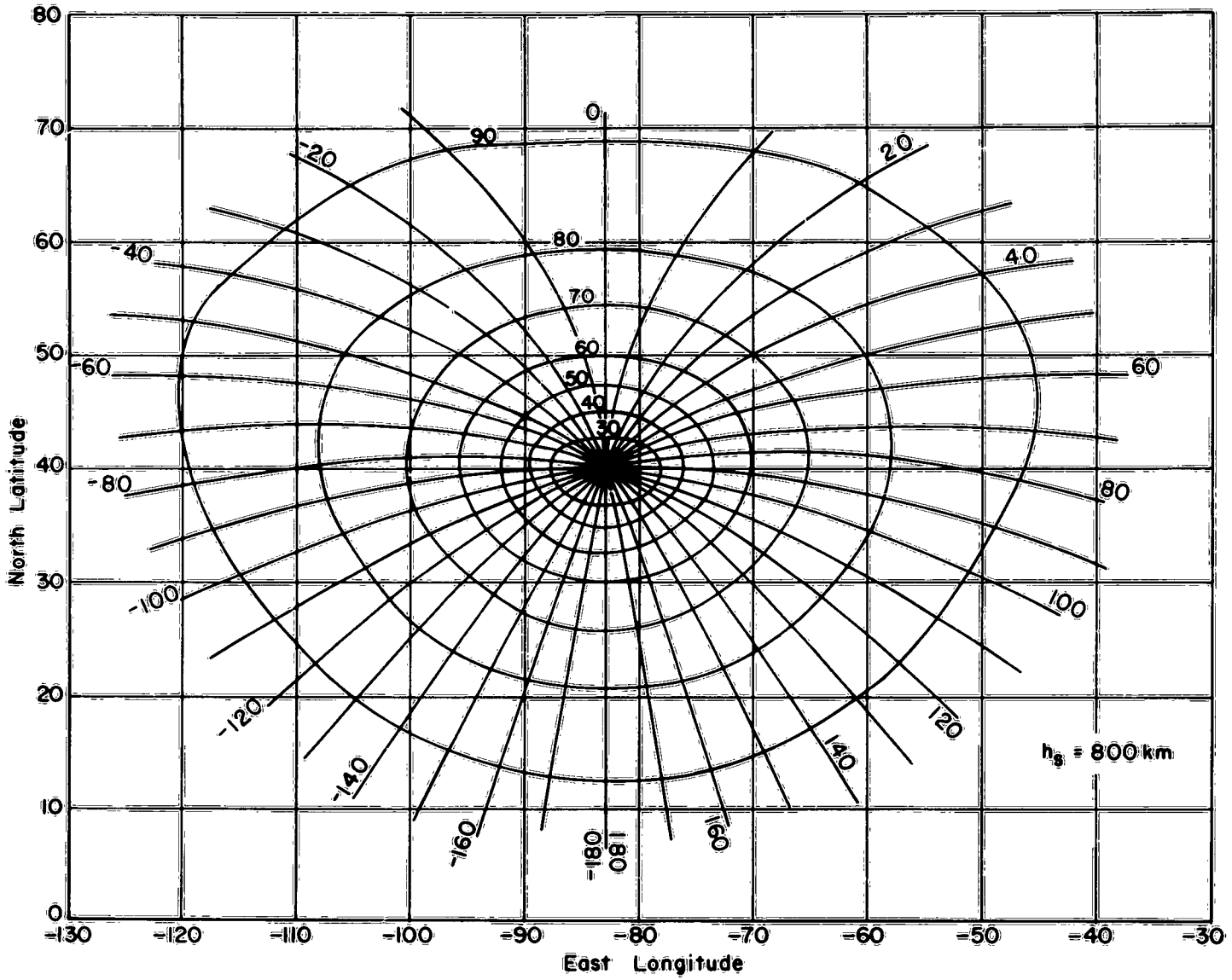

Fig. 21b. az-Va 800.

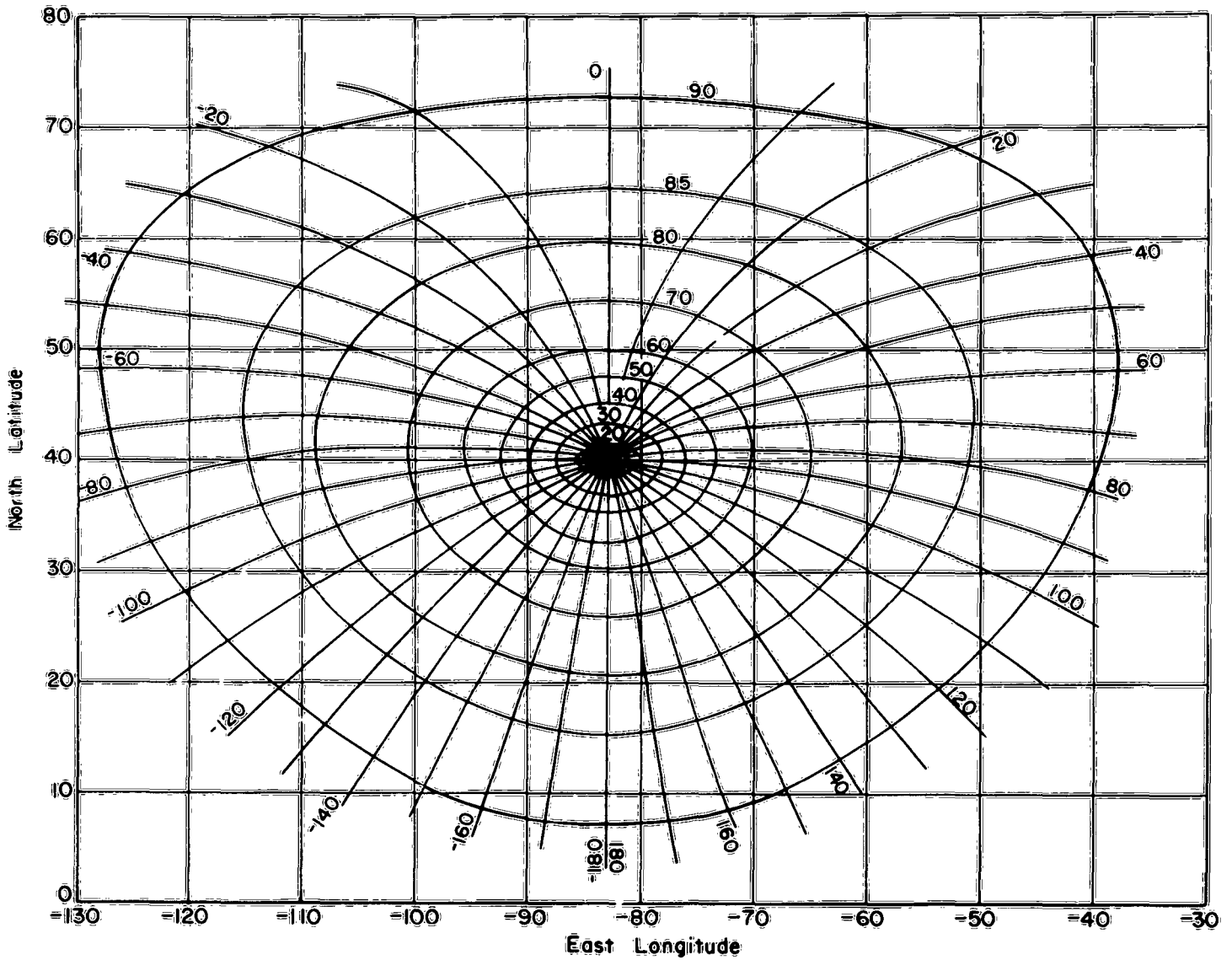

Fig. 21c. az-Va 1200.

APPENDIX IV - AN EXPANSION OF THE EARTH'S MAGNETIC FIELD

An important factor in determining the Faraday rotation of a satellite signal is a knowledge of the magnitude and direction of the magnetic field along the propagation path. Furthermore, when the rate of Faraday rotation is of interest, the relative magnitudes and directions between two points must be known quite accurately. The earth's magnetic field, therefore, was expanded in spherical harmonics using coefficients which match measured values of the magnetic field at the earth's surface. The formulation of the expressions used were originally those of Gauss, however the recent work of Jones and Melotte[41] is used directly.

Assuming no sources of the magnetic field external to the earth, the magnetic potential expressed in spherical harmonics is given by:

$$(6.2) \quad V_H = a \sum_{n=1}^{\infty} \sum_{m=0}^{n} \left(\frac{a}{r}\right)^{n+1} H_n^m (\sin\lambda)(g_n^m \cos m\phi + h_n^m \sin m\phi)$$

where in a right-handed system of geocentric coordinates

V = magnetic potential

a = radius of the earth

r = the radial distance from the center of the earth to a field point

λ = latitude

ϕ = longitude

$$H_n^m = \frac{2^n n!\,(n-m)!}{(2n)!} P_n^m(\cos\theta)$$

$P_n^m(\cos\theta)$ = the associated Legendre Polynomials

θ = geographic co-latitude

g_n^m and h_n^m = the constant Gaussian coefficients determined from surface magnetic data.

The magnetic field components are found from the magnetic potential as follows: the northerly component is

$$(63)\quad H_x = \frac{1}{r}\frac{\partial V}{\partial \lambda} = \sec\lambda \sum_{n=1}^{\infty}\sum_{m=0}^{n}\left(\frac{a}{r}\right)^{n+2}\cos\lambda\,\frac{dH_n^m}{d\lambda}\,(g_n^m\cos m\phi + h_n^m\sin m\phi);$$

the easterly component is

$$(64)\quad H_y = \frac{1}{r\cos\lambda}\,\frac{\partial V}{\partial \phi} = \sec\lambda \sum_{n=1}^{\infty}\sum_{m=0}^{n}\left(\frac{a}{r}\right)^{n+2} mH_n^m\,(-g_n^m\sin m\phi + h_n^m\cos m\phi);$$

the downward component is

$$(65)\quad H_z = -\frac{\partial V}{\partial r} = \sum_{n=1}^{\infty}\sum_{m=0}^{n}(n+1)H_n^m\,(g_n^m\cos m\phi + h_n^m\sin m\phi).$$

Thus, at any point above the earth's surface the magnetic field is described by three vectors.

The Gaussian coefficients used here are tabulated in Table II and are taken from the work of Finch and Leaton.[42] The coefficients have the same units as the magnetic field in the M.K.S. system (amperes per meter).

The quantity M is defined as

$$M \equiv |\underline{H}|\cos\phi\sec\xi$$

and values of M are shown in Fig. 22 as a function of vertical angle and azimuth angle for three different heights.

TABLE II

GAUSSIAN COEFFICIENTS IN M.K.S.

g_n^m

n \ m	0	1	2	3	4	5	6
1	+24.307	+2.1207					
2	+ 1.8144	-4.1738	-1.0902				
3	- 2.3475	+4.6592	-1.9457	-.57296			
4	- 3.3184	-3.5014	-1.7984	+.63264	-.18303		
5	+ 1.6194	-2.5743	-1.2334	+.15120	+.27056	+.03979	
6	- 1.1897	- .79975	- .15120	-1.8701	+.13130	-.00796	+.05570

h_n^m

n \ m	0	1	2	3	4	5	6
1		-4.7030					
2		+2.6221	-.17109				
3		+1.1061	-.44961	+.06366			
4		-.64458	+.94300	+.06366	+.09549		
5		-.14722	-.56898	+.16711	+.25067	-.04775	
6		+.39391	-1.3648	.00000	+.04377	+.04775	+.00796

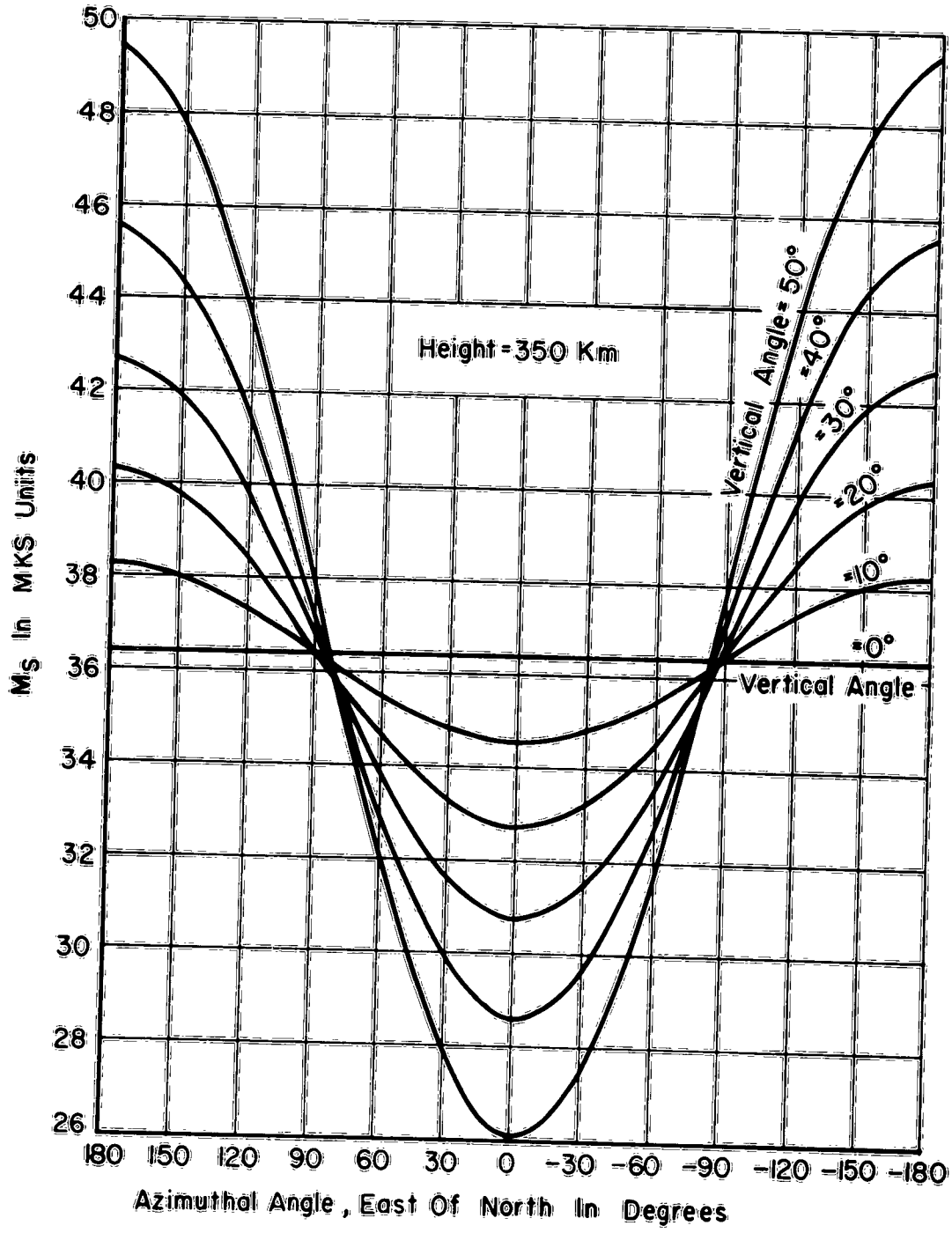
50
48
46
44
42
40
38
36
34
32
30
28
26
M_S In MKS Units
Height = 350 Km
Vertical Angle = 50°
= 40°
= 30°
= 20°
= 10°
= 0°
Vertical Angle
180 150 120 90 60 30 0 -30 -60 -90 -120 -150 -180
Azimuthal Angle, East Of North In Degrees

Fig. 22a. M 350.

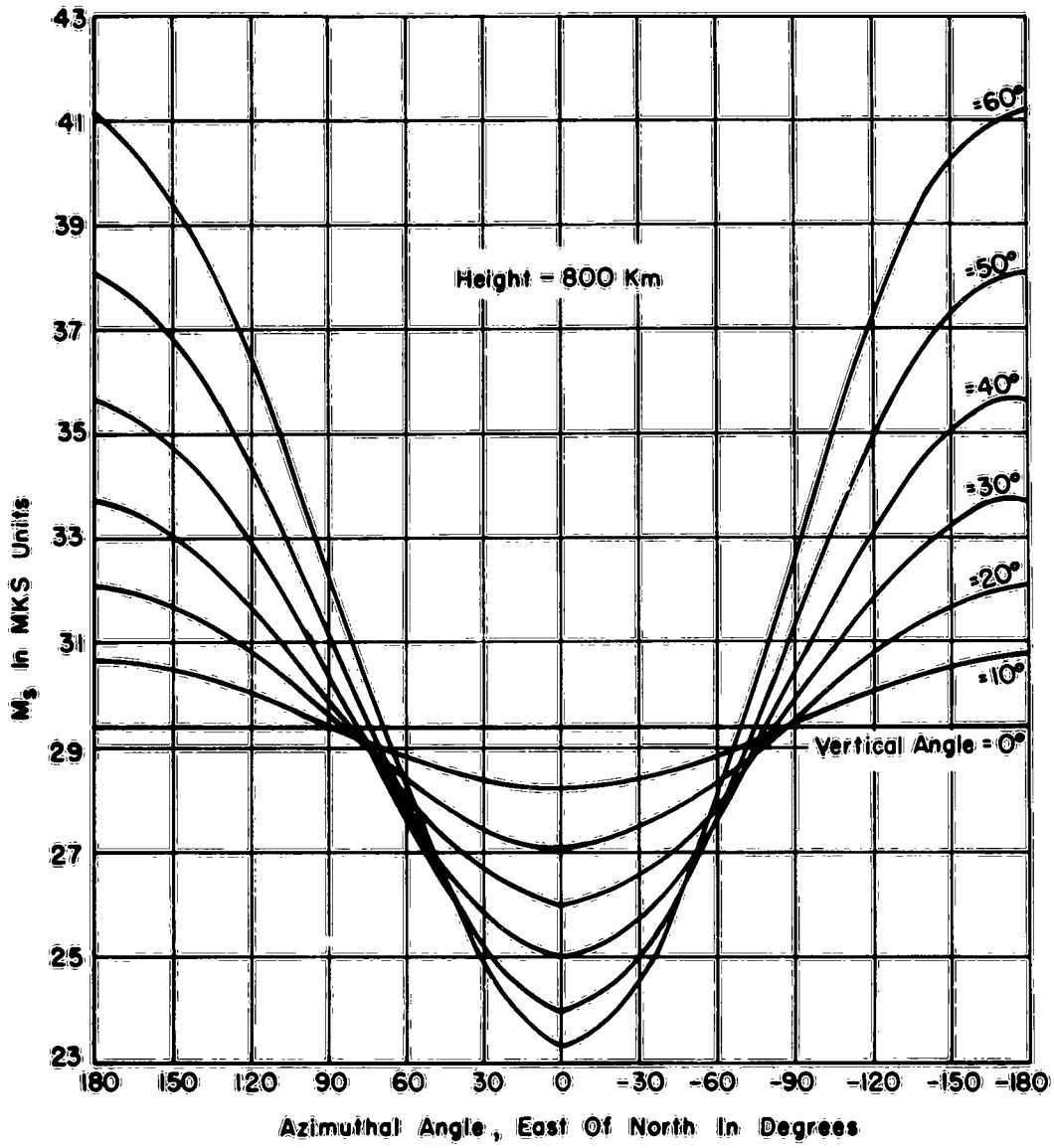
43
41
39
37
35
33
31
29
27
25
23
M_s In MKS Units
Height = 800 Km
=60°
=50°
=40°
=30°
=20°
=10°
Vertical Angle = 0°
180
150
120
90
60
30
0
-30
-60
-90
-120
-150
-180
Azimuthal Angle, East Of North In Degrees

Fig. 22b. M 800.

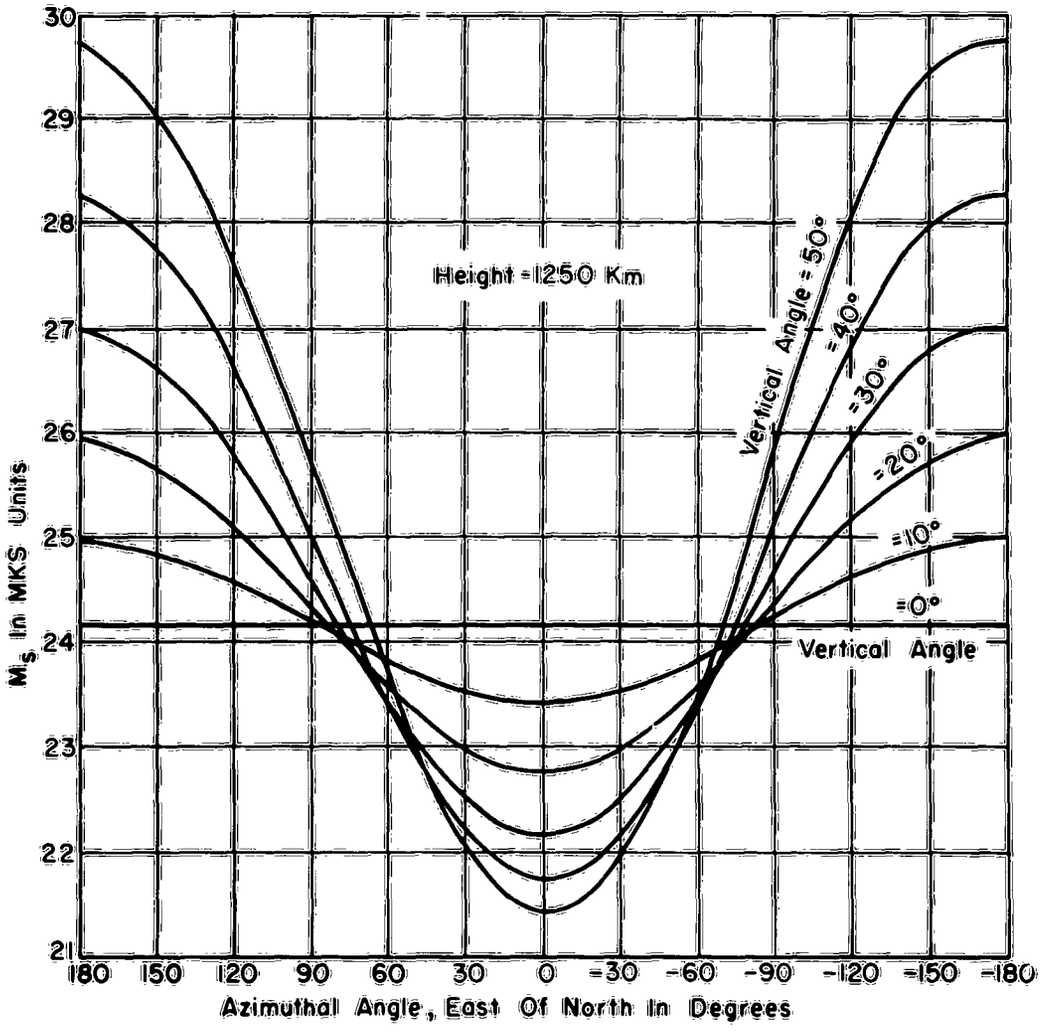

Fig. 22c. M 1200.

APPENDIX V - DISCUSSION OF THE MEAN VALUES $\overline{M}$, h_M

Given the first order equation for θ, the total polarization rotation, in the form:

$$(66) \quad \theta = \frac{K_1}{f^2} \int_0^{h_s} M N \, dh ,$$

it is of interest to separate the integrated electron density to the satellite;

$$N_H = \int_0^{h_s} N \, dh ,$$

from the remaining functions in order to solve for N_H algebraically. At a single frequency, the most obvious method of accomplishing this separation is by the mean value procedure. That is, under certain conditions there is a mean value of M, $\overline{M}$, which exists defined by

$$(67) \quad \overline{M} \int_0^{h_s} N \, dh = \int_0^{h_s} MN \, dh;$$

or, in another form

$$(68) \quad \overline{M} = \frac{\int_0^{h_s} MN \, dh}{\int_0^{h_s} N \, dh} .$$

In evaluating $\overline{M}$, it has been found necessary that M(h) and N(h) be known, greater than zero and have continuous derivatives for all positive values of h. M(h) is known from Appendix IV and the geometrical quantities of Appendix III. N(h) which, in general, is a diurnally, seasonally, and sunspot-cyclically varying function must be assumed for this purpose. The assumed noon-time average distribution is shown in Fig. 6b and it is based on measurements by Hame.[24] Since the actual N(h) is known to have a maximum which drifts slightly in

height while maintaining the same general shape, it may be said the final values for $\overline{\overline{M}}$ are relatively insensitive to the exact N(h) model assumed.

On carrying out the calculations outlined above using the distribution of N(h) shown in Fig. 3a, mean values, $\overline{\overline{M}}(h_s)$, were found for the three cases: overhead, 30° from overhead looking south, and 30° from overhead looking north. The values of $\overline{\overline{M}}(h_s)$ found are the same as those at some particular height, h_m, called the mean height. The results are more meaningful if one plots the mean heights as a function of the actual heights as shown in Fig. 23. Thus, whenever the total polarization rotation is known a representative figure for N_H may be obtained by evaluating $\overline{\overline{M}}$ at the appropriate mean height corresponding to the actual satellite height, and N_H is given by

$$(69) \quad N_H = \frac{\theta \cdot f^2}{\overline{\overline{M}}(h_m) \cdot K_1}$$

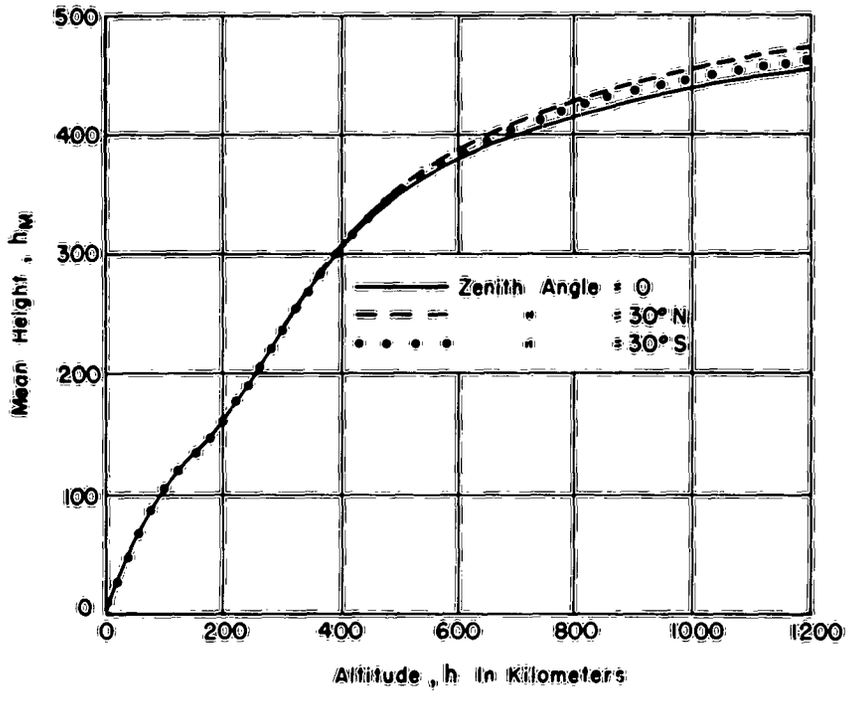

Fig. 23. The mean height h_m, as a function of altitude.

APPENDIX VI - EXPERIMENTAL EQUIPMENT

The equipment used in recording the radio transmission of Explorer VII (1959 Iota I) is quite simple, and this description is included only for the sake of completeness.

Figure 24a shows a block diagram of the measuring system. The orthogonal folded dipoles in Fig. 24b were used in order to separate Faraday rotation of the signal from spurious amplitude fluctuations. This is possible because a null on one dipole occurs at the same time as a peak on the other dipole when the satellite is directly overhead. Thus any peaks or nulls occuring simultaneously on both dipoles can be eliminated as amplitude fluctuations.

The antennas are folded dipoles connected to 50-ohm coaxial lead-in cable through a 4-to-1 balun in order to eliminate any current flow on the outer conductor of the lead-in cable.

Figure 25 shows the 108 Mc interferometer lined up exactly east-west in order to obtain a null along the meridian 83° 02' W. The two antennas are the same as discussed above. The 108 Mc interferometer pattern in an east-west plane is shown in Fig. 26, assuming a perfectly conducting earth.

Figure 27 shows the equipment panel of receivers, preamplifiers, integrating circuits, and the recorder. The receivers used were Collins Model 51J4, set on a bandwidth of 3 kilocycles. The recorder is a 4-channel Sanborn with recording speeds from 0.25 mm/sec to 100 mm/sec.

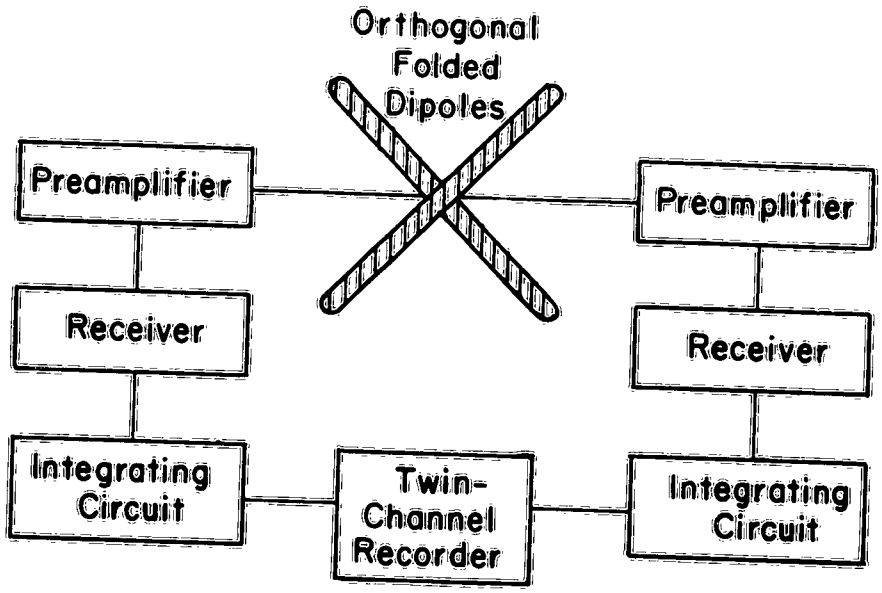

Fig. 24a. Block diagram.

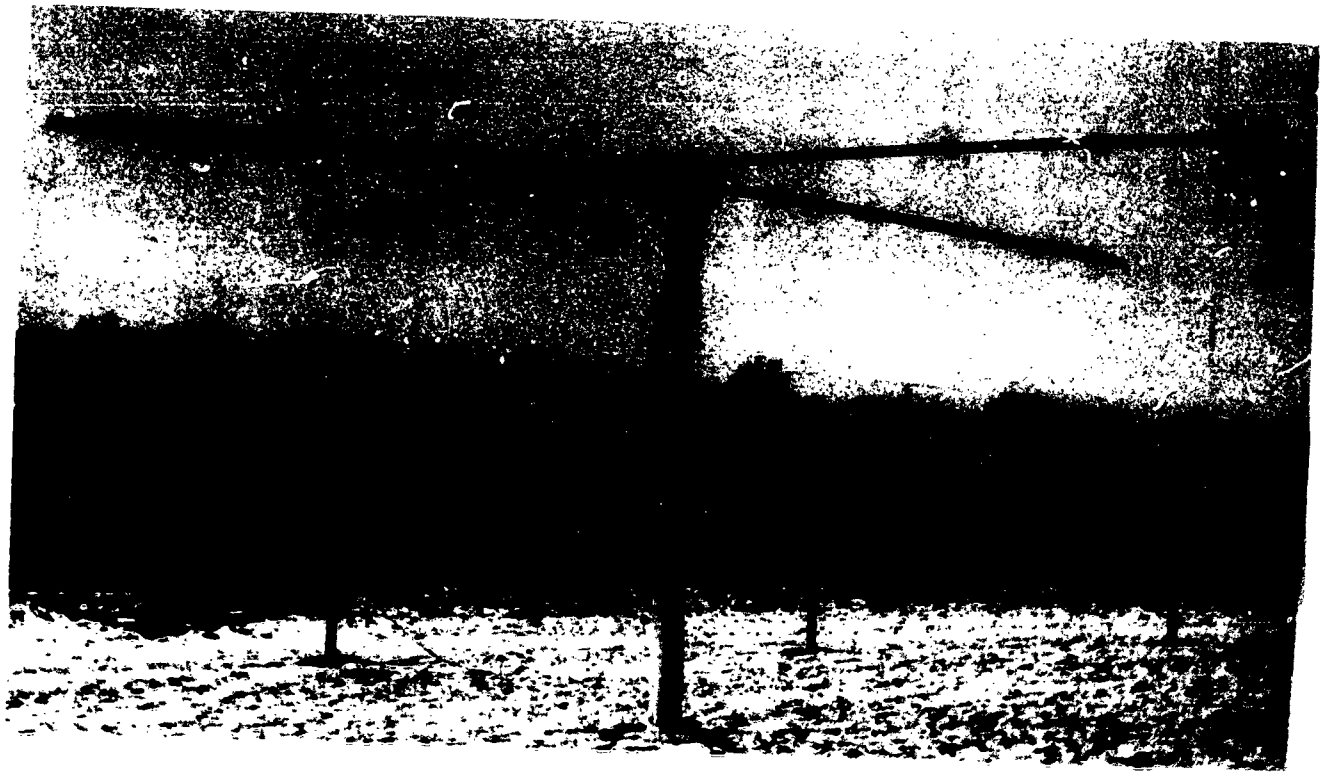

Fig. 24b. Dipoles.

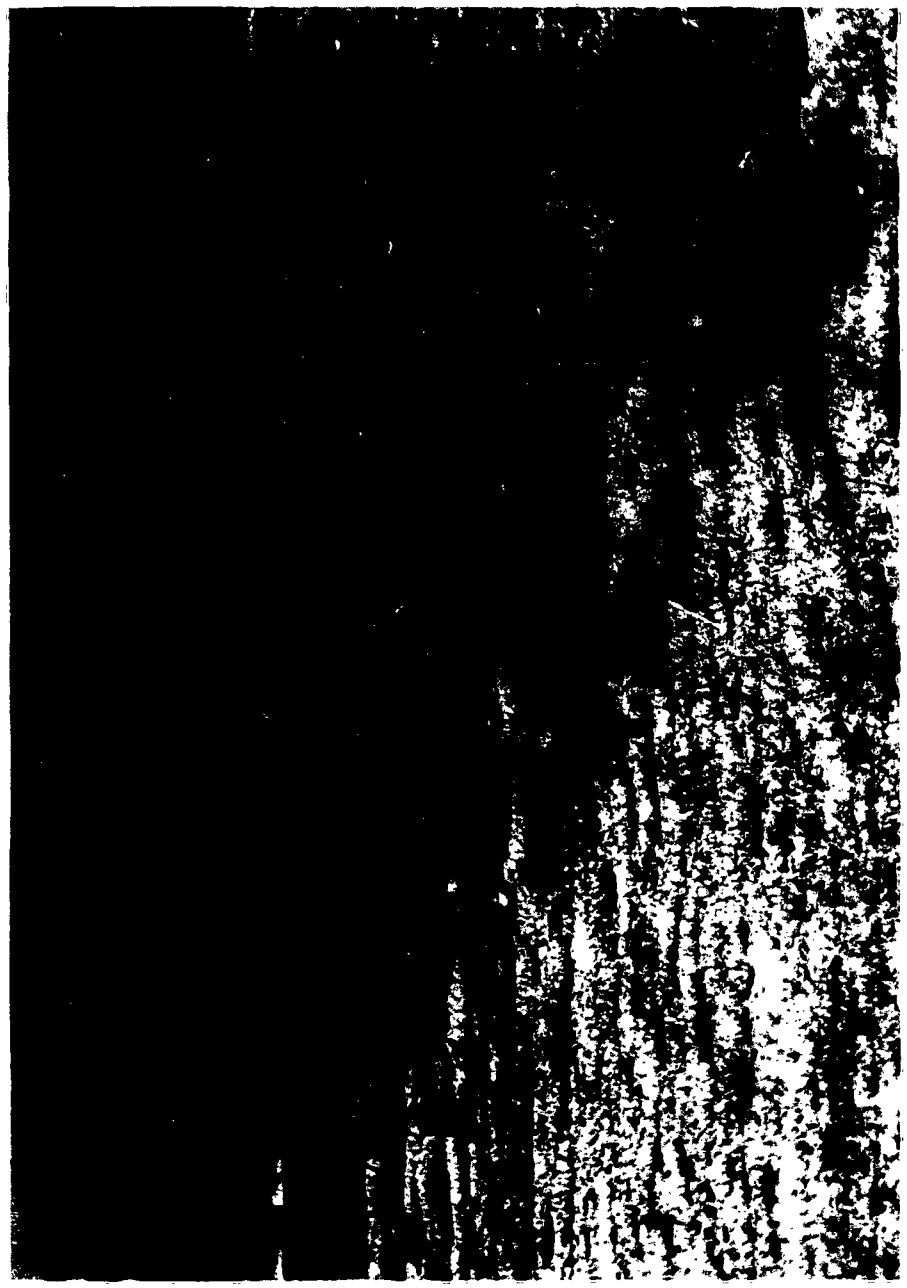

Fig. 25. 108 mc interferometer.

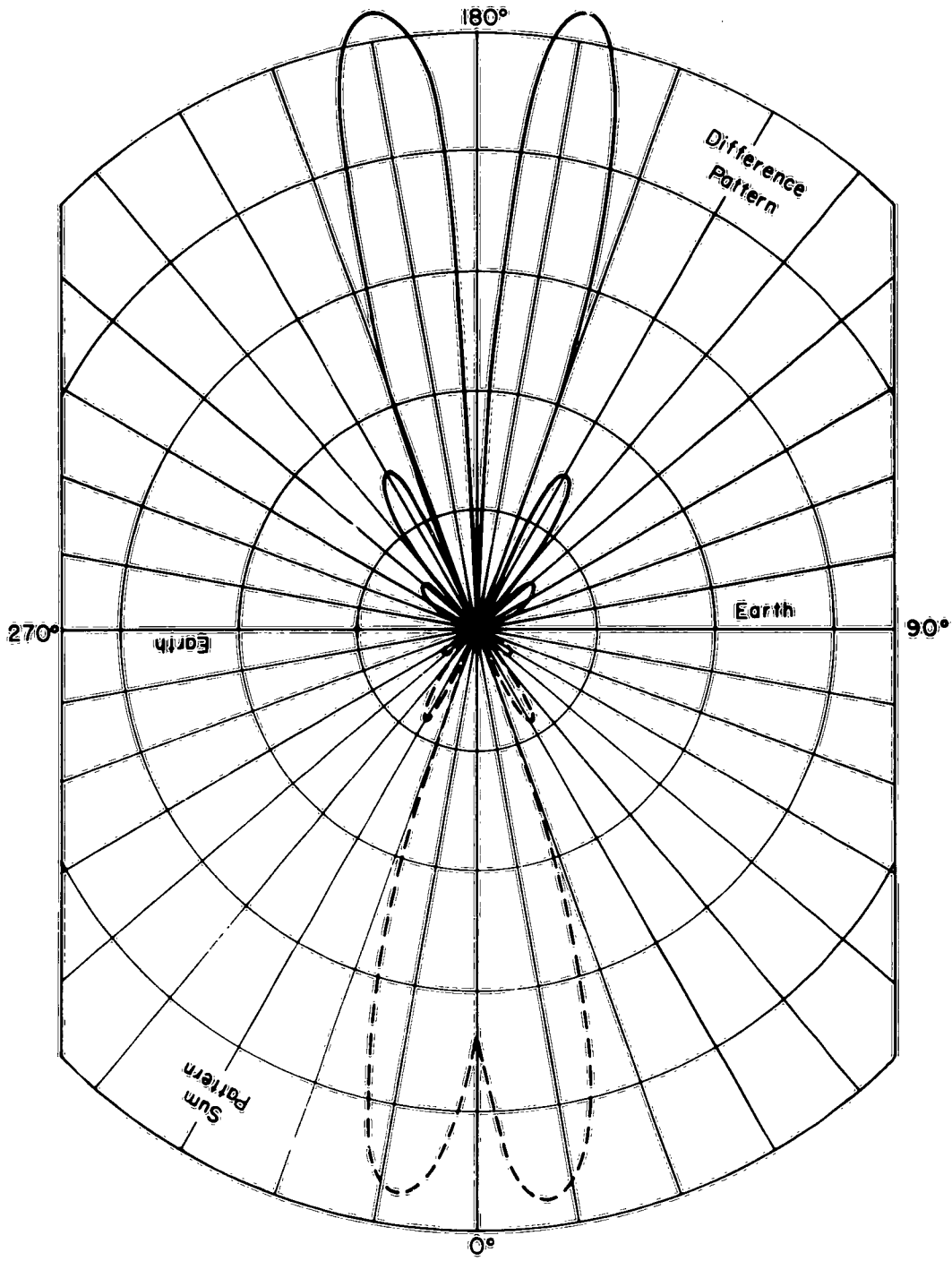

Fig. 26. Interferometer pattern.

Fig. 27. Receivers, recorders, etc.

PROJECT 1116
REPORTS DISTRIBUTION LIST
CONTRACT AF 19(604)-7270

Code	Organization	No. of Copies
AF 5	AFMTC (AFMTC Tech Library-MU-135) Patrick AFB, Fla.	1
AF 18	AUL Maxwell AFB, Ala.	1
AF 43	ASD (ASAPRD-Dist) Wright-Patterson AFB, Ohio	1
AF 91	AFOSR (SRGL) Washington 25, D. C.	1
AF 124	RADC(RAYLD) Griffiss AFB, New York Attn: Documents Library	1
AF 139	AF Missile Development Center (MDGRT) Holloman AFB, New Mexico	1
AF 318	ARL (Technical Library) Building 450 Wright-Patterson AFB, Ohio	1
AR 5	Commanding General USASRDL Ft. Monmouth, N. J. Attn: Tech. Doc. Ctr. SLGRA/SL-ADT	1
Ar 9	Department of the Army Office of the Chief Signal Officer Washington 25, D. C. SIGRD-4a-2	1
Ar 50	Commanding Officer Attn: ORDTL-012 Diamond Ordnance Fuze Laboratories Washington 25, D. C.	1
Ar 67	Army Rocket and Guided Missile Agency Redstone Arsenal, Ala. Attn: ORDXR-OTL, Technical Library	1

Code	Organization	No. of Copies
G2	ASTIA (TIPAA) Arlington Hall Station Arlington 12, Virginia	10
G 68	National Aeronautics and Space Agency 1520 H Street, N. W. Washington 25, D. C. Attn: Library	1
G 109	Director Langley Research Center National Aeronautics and Space Administration Langley Field, Virginia	1
M 6	AFCRL, OAR(CRIPA- Stop 39) L. G. Hanscom Field Bedford, Massachusetts	10
M 78	AFCRL, OAR(CRT, Dr. A. M. Gerlach) L. G. Hanscom Field Bedford, Massachusetts	1
N 9	Chief, Bureau of Naval Weapons Department of the Navy Washington 25, D. C. (Attn: DLI-31)	2
N 29	Director (Code 2027) U. S. Naval Research Laboratory Washington 25, D. C.	2
I 292	Director, USAF Project RAND The Rand Corporation 1700 Main Street Santa Monica, California Thru: A. F. Liaison Office	1
AF 253	Technical Information Office European Office, Aerospace Research Shell Building, 47 Cantersteen Brussels, Belgium	1
Ar 107	U. S. Army Aviation Human Research Unit U. S. Continental Army Command P. O. Box 428 Fort Rucker, Alabama Attn: Major Arne H. Eliasson	1

Code	Destination	No. of Copies
G 8	Library Boulder Laboratories National Bureau of Standards Boulder, Colorado	2
M 63	Institute of the Aerospace Sciences, Inc. 2 East 64th Street New York 21, New York Attn: Librarian	1
N 73	Office of Naval Research Branch Office, London Navy 100, Box 39 F.P.O. New York, N.Y.	10
U 32	Massachusetts Institute of Technology Research Laboratory of Electronics Building 26, Room 327 Cambridge 39, Massachusetts Attn: John H. Hewitt	1
U 431	Alderman Library University of Virginia Charlottesville, Virginia	1
AF 68	ASD (ASRNRE-3/Mr. Paul W. Springer) Wright-Patterson AFB, Ohio	1
AF 249	AF Missile Test Center (MTTR, Mr. Carol Schory) Directorate of Special Tests Patrick AFB, Fla.	1
AF 295	SAC (OASCI) Offutt AFB, Nebraska	1
AF 296	RADC (RCLTT, Mr. Frank Bradley) Griffiss AFB, N.Y.	1
AF 337	Hq. USAF (AFDFD, Lt. Col. Fred Jones) Pentagon, Washington 25, D.C. "for transmission to: SHAPE, ADTC, Dr. Max R. Nagel"	1
AF 297	RADC (RCU, Mr. George Brunetti) Griffiss AFB, New York	1

Code	Organization	No. of Copies
AF 343	Hq. AFSC (SCRC) Attn: Major Alfred D. Blue Washington 25, D.C.	1
G 18	Office of the Assistant Secretary of Defense (R&D) Washington 25, D.C. Attn: Office of Electronics	1
G 96	Institute for Defense Analysis/Dr. Paul Von Handel Universal Building 1825 Connecticut Avenue, N.W. Washington, D.C.	1
G 119	ARPA (Mr. Fred A. Koether) Washington 25, D.C.	2
I 128	Raytheon Company 225 Crescent Street Waltham, Mass. Attn: Mr. D. A. Hedlund Communications & Data Processing Operation	1
I 225	Pickard & Burns Inc. 240 Highland Avenue Needham 94, Mass. Attn: Dr. Richard H. Woodward	1
I 648	The Mitre Corporation 244 Wood Street Lexington 73, Mass. Attn: Mrs. Jean E. Claflin, Librarian	1
I 702	The Rand Corporation 1700 Main Street Santa Monica, California Attn: Dr. Cullen Crain	1
I 795	Bendix Aviation Corp. Systems Division 3300 Plymouth Road Ann Arbor, Michigan Attn: Dr. Otho Lyle Tiffany	1

Code	Organization	No. of Copies
I 796	Stanford Research Institute Menlo Park, California Attn: Lambert T. Dolphin	1
I 798	Reaction Motors Division Thiokol Chemical Corporation Denville, New Jersey Attn: H. G. Wolfhard	1
I 803	ACF Industries, Inc. ERCO Div. 4705 Queensbury Road Riverdale, Maryland Attn: Mr. William Whelan	1
I 935	Stanford Research Institute Menlo Park, California Attn: Mr. Donald Nielson	1
M 70	ESD (ESRDT, Mr. H. Byram) L. G. Hanscom Field Bedford, Mass.	1
M 73	ESD (ESSIB, Mr. Richard McManus) L. G. Hanscom Field Bedford, Mass.	1
N 133	Director U. S. Naval Research Laboratory Washington 25, D. C. Attn: Mr. W. W. Balwanz	1
N 146	Office of Naval Research Department of the Navy Washington 25, D. C. Attn: Code 418	1
N 154	Commanding Officer U. S. Naval Ordnance Laboratory Corona, California Attn: Mr. D. Hildebrand	1

Code	Organization	No. of Copies
U 26	Massachusetts Institute of Technology Lincoln Laboratory P. O. Box 73 Lexington 73, Massachusetts Attn: Mary A. Granese, Librarian	1
U 79	University of Michigan Engineering Research Institute Radiation Laboratory 912 N. Main Street Ann Arbor, Michigan Attn: Prof. K. M. Siegel	1
U 84	Stanford Electronics Laboratories Stanford University Stanford, California Attn: Dr. Oswald G. Villard, Jr. Radio Science Laboratory	1
U 89	Stanford Electronics Laboratories Stanford University Stanford, California Attn: Dr. Robert A. Helliwell Radio Science Laboratory	1
U 372	The University of Michigan Willow Run Laboratories P. O. Box 2008 Ann Arbor, Michigan Attn: B. R. George, BAMIRAC Library	1
U 422	Massachusetts Institute of Technology Lincoln Laboratory P. O. Box 73 Lexington 73, Massachusetts Attn: Dr. Martin Balser	1
	AFCRL, Office of Aerospace Research (CRRI) L. G. Hanscom Field Bedford, Massachusetts	10